












SOURCE  
DATATRANSPARENT  
PROCESSOPEN  
ACCESS

# LUBAC assembles a ubiquitin signaling platform at mitochondria for signal amplification and transport of NF- $\kappa$ B to the nucleus

Zhixiao Wu<sup>1,†</sup> , Lena A Berlemann<sup>1,†</sup>, Verian Bader<sup>1,2,‡</sup> , Dominik A Sehr<sup>1,‡</sup>, Eva Dawin<sup>1,3,‡</sup>, Alberto Covallero<sup>4,‡</sup>, Jens Meschede<sup>1</sup>, Lena Angersbach<sup>1</sup>, Cathrin Showkat<sup>1</sup>, Jonas B Michaelis<sup>5</sup> , Christian Münch<sup>5</sup> , Bettina Rieger<sup>6</sup>, Dmitry Namgaladze<sup>7</sup>, Maria Georgina Herrera<sup>1</sup>, Fabienne C Fiesel<sup>8,9</sup>, Wolfdieter Springer<sup>8,9</sup> , Marta Mendes<sup>10</sup>, Jennifer Stepien<sup>11,12</sup>, Katalin Barkovits<sup>11,12</sup>, Katrin Marcus<sup>11,12</sup>, Albert Sickmann<sup>3</sup>, Gunnar Dittmar<sup>10,13</sup> , Karin B Busch<sup>6</sup>, Dietmar Riedel<sup>14</sup> , Marisa Brini<sup>15,16</sup> , Jörg Tatzelt<sup>2,17</sup> , Tito Cali<sup>4,16,18</sup>  & Konstanze F Winklhofer<sup>1,17,\*</sup> 

## Abstract

Mitochondria are increasingly recognized as cellular hubs to orchestrate signaling pathways that regulate metabolism, redox homeostasis, and cell fate decisions. Recent research revealed a role of mitochondria also in innate immune signaling; however, the mechanisms of how mitochondria affect signal transduction are poorly understood. Here, we show that the NF- $\kappa$ B pathway activated by TNF employs mitochondria as a platform for signal amplification and shuttling of activated NF- $\kappa$ B to the nucleus. TNF treatment induces the recruitment of HOIP, the catalytic component of the linear ubiquitin chain assembly complex (LUBAC), and its substrate NEMO to the outer mitochondrial membrane, where M1- and K63-linked ubiquitin chains are generated. NF- $\kappa$ B is locally activated and transported to the nucleus by mitochondria, leading to an increase in mitochondria-nucleus contact sites in a HOIP-dependent manner. Notably, TNF-induced stabilization of the mitochondrial kinase PINK1 furthermore contributes to signal amplification by

antagonizing the M1-ubiquitin-specific deubiquitinase OTULIN. Overall, our study reveals a role for mitochondria in amplifying TNF-mediated NF- $\kappa$ B activation, both serving as a signaling platform, as well as a transport mode for activated NF- $\kappa$ B to the nuclear.

**Keywords** HOIP; NEMO; OTULIN; PINK1; ubiquitin

**Subject Categories** Post-translational Modifications & Proteolysis; Signal Transduction

**DOI** 10.15252/emboj.2022112006 | Received 29 June 2022 | Revised 20 October 2022 | Accepted 25 October 2022 | Published online 18 November 2022

**The EMBO Journal (2022) 41: e112006**

See also: [J Chen & T Simmen](#) (December 2022)

## Introduction

In addition to their bioenergetic and biosynthetic functions, mitochondria have emerged as potent and versatile signaling organelles

- 1 Department Molecular Cell Biology, Institute of Biochemistry and Pathobiochemistry, Ruhr University Bochum, Bochum, Germany
- 2 Department Biochemistry of Neurodegenerative Diseases, Institute of Biochemistry and Pathobiochemistry, Ruhr University Bochum, Bochum, Germany
- 3 Leibniz-Institut für Analytische Wissenschaften—ISAS—e.V, Dortmund, Germany
- 4 Department of Biomedical Sciences, University of Padua, Padua, Italy
- 5 Faculty of Medicine, Institute of Biochemistry II, Goethe University Frankfurt, Frankfurt am Main, Germany
- 6 Institute for Integrative Cell Biology and Physiology, Faculty of Biology, University of Münster, Münster, Germany
- 7 Institute of Biochemistry I, Faculty of Medicine, Goethe-University Frankfurt, Frankfurt, Germany
- 8 Department of Neuroscience, Mayo Clinic, Jacksonville, FL, USA
- 9 Neuroscience PhD Program, Mayo Clinic Graduate School of Biomedical Sciences, Jacksonville, FL, USA
- 10 Proteomics of Cellular Signaling, Department of Infection and Immunity, Luxembourg Institute of Health, Strassen, Luxembourg
- 11 Medizinisches Proteom-Center, Ruhr-Universität Bochum, Bochum, Germany
- 12 Medical Proteome Analysis, Center for Protein Diagnostics (PRODI), Ruhr-Universität Bochum, Bochum, Germany
- 13 Department of Life Sciences and Medicine, University of Luxembourg, Belvaux, Luxembourg
- 14 Laboratory for Electron Microscopy, Max Planck Institute for Multidisciplinary Sciences, Göttingen, Germany
- 15 Department of Biology, University of Padua, Padua, Italy
- 16 Centro Studi per la Neurodegenerazione (CESNE), University of Padua, Padua, Italy
- 17 RESOLV Cluster of Excellence, Ruhr University Bochum, Bochum, Germany
- 18 Padua Neuroscience Center (PNC), University of Padua, Padua, Italy

\*Corresponding author. Tel:+49 234 3228428; E-mail: konstanze.winklhofer@rub.de

<sup>†</sup>These authors contributed equally to this work

<sup>‡</sup>These authors contributed equally to this work

to adapt metabolism to cellular demands, to communicate mitochondrial fitness to other cellular compartments, and to regulate cell death and viability (Nunnari & Suomalainen, 2012; Weinberg et al, 2015; Youle, 2019; Bock & Tait, 2020; Giacomello et al, 2020; Tiku et al, 2020; Bahat et al, 2021; Cervantes-Silva et al, 2021). Increasing evidence implicates mitochondria in innate immune signaling, illustrating that mitochondria have been co-opted by eukaryotic cells to react to cellular damage and to promote efficient immune responses. For example, invading pathogens expose pathogen-associated molecular patterns (PAMPs), such as viral RNA, which is recognized by cytoplasmic RLRs (retinoic acid-inducible gene-I-like receptors). Binding of viral RNA to RLRs induces a conformational change, allowing their recruitment to the mitochondrial RLR adaptor protein MAVS (mitochondrial antiviral signaling protein). Subsequent multimerization of MAVS at mitochondria results in the activation of the transcription factors IRF (interferon-regulatory factor) 3, IRF7, and NF- $\kappa$ B (nuclear factor-kappaB), which regulate the expression of type 1 interferons and proinflammatory cytokines (Seth et al, 2005; Ablasser & Hur, 2020; Rehwinkel & Gack, 2020; Chowdhury et al, 2022).

NF- $\kappa$ B is activated in several innate immune paradigms and is well known for its role in pathological conditions, where prolonged or profuse NF- $\kappa$ B activation in reactive immune or glial cells causes inflammation. However, NF- $\kappa$ B has important physiological functions in most—if not all—cell types. In the nervous system, NF- $\kappa$ B maintains neuronal viability and regulates synaptic plasticity (Meffert et al, 2003; O’Riordan et al, 2006; Salles et al, 2015; Neidl et al, 2016; Dresselhaus et al, 2018). Constitutive NF- $\kappa$ B activation by para- or autocrine loops is required for neuronal survival, and stress-induced transient NF- $\kappa$ B activation confers protection from various neurotoxic insults (Blondeau et al, 2001; Bhakar et al, 2002). Accordingly, TNF has been identified as a neuroprotective cytokine that prevents neuronal damage under various stress conditions (Cheng et al, 1994; Turrin & Rivest, 2006).

Although TNF can induce apoptotic or necroptotic cell death in certain pathological conditions, it usually protects from cell death. Engagement of TNF with its receptor TNFR1 at the plasma membrane results in the formation of signaling complex I that activates the transcription factor NF- $\kappa$ B (typically p65/p50 heterodimers) in a tightly regulated manner, involving multiple phosphorylation and ubiquitination events (Hayden & Ghosh, 2014; Brenner et al, 2015; Annibaldi & Meier, 2018; Varfolomeev & Vucic, 2018). A crucial step in the activation process is the ubiquitination of NEMO (NF- $\kappa$ B essential modulator) by HOIP, the catalytic component of the linear ubiquitin chain assembly complex (LUBAC), and binding of NEMO to linear ubiquitin chains by its UBAN (ubiquitin-binding domain in ABIN and NEMO) domain (Haas et al, 2009; Rahighi et al, 2009; Tokunaga et al, 2009; Fujita et al, 2014). These events induce a conformational change and oligomerization of NEMO, activating the associated kinases IKK $\alpha$  and IKK $\beta$ . IKK $\alpha$ / $\beta$  phosphorylates the NF- $\kappa$ B inhibitor I $\kappa$ B $\alpha$ , which is subsequently modified by K48-linked ubiquitin chains and degraded by the proteasome. NF- $\kappa$ B heterodimers, liberated from their inhibitory binding to I $\kappa$ B $\alpha$ , are then translocated from the cytoplasm to the nucleus, where they increase the expression of anti-apoptotic proteins or proinflammatory cytokines in a cell type- and context-specific manner.

We have previously shown that the E3 ubiquitin ligase Parkin depends on this pathway to protect from stress-induced neuronal cell death (Henn et al, 2007; Muller-Rischart et al, 2013). Parkin modifies NEMO with K63-linked ubiquitin chains and facilitates subsequent M1-linked ubiquitination of NEMO by HOIP, supporting the concept that linear ubiquitin chains are preferentially assembled as heterotypic K63/M1-linked chains in innate immune signaling pathways (Emmerich et al, 2013, 2016; Fiil et al, 2013; Hrdinka et al, 2016; Cohen & Strickson, 2017). Notably, in the absence of either HOIP or NEMO, Parkin cannot prevent stress-induced cell death (Muller-Rischart et al, 2013).

Linear or M1-linked ubiquitination is characterized by the head-to-tail linkage of ubiquitin molecules via the C-terminal carboxyl group of the donor ubiquitin and the N-terminal methionine of the acceptor ubiquitin (Kirisako et al, 2006; Dittmar & Winklhofer, 2019; Spit et al, 2019; Oikawa et al, 2020; Fiil & Gyrd-Hansen, 2021; Fuseya & Iwai, 2021; Jahan et al, 2021; Shibata & Komander, 2022; Tokunaga & Ikeda, 2022). Formation and disassembly of linear ubiquitin chains are highly specific processes. HOIP is the only E3 ubiquitin ligase that generates linear ubiquitin chains, whereas OTULIN is the only deubiquitinase that exclusively hydrolyses linear ubiquitin chains (Keusekotten et al, 2013; Rivkin et al, 2013; Lork et al, 2017; Verboom et al, 2021; Weinelt & van Wijk, 2021). Thus, M1-linked ubiquitination can be studied with unique specificity, in contrast to other types of ubiquitination. Mass spectrometry data on TNF-induced signaling networks and the interactive profile of HOIP and OTULIN directed our interest toward mitochondria (Wagner et al, 2016; Kupka et al, 2016a; Stangl et al, 2019). Here we show that TNF induces remodeling of the outer mitochondrial membrane by assembling an NF- $\kappa$ B signaling platform that facilitates nuclear translocation of activated NF- $\kappa$ B. HOIP plays a crucial role in this process by generating M1-linked ubiquitin chains and stabilizing the mitochondrial kinase PINK1, which contributes to NF- $\kappa$ B signal amplification through the phosphorylation of ubiquitin.

## Results

### TNF induces recruitment of LUBAC and the assembly of linear ubiquitin chains at mitochondria

To get insight into the subcellular localization of OTULIN and its interactive profile, we performed co-immunoprecipitation of HA-tagged OTULIN expressed in HEK293T cells coupled to mass spectrometry. Strict filtering criteria were applied in two independent experiments, including only proteins, which were detected by at least two unique peptides that were not present in the negative controls. By this approach, 59 potential OTULIN-interacting proteins were identified (Appendix Fig S1A). An analysis of the subcellular localization of OTULIN-interacting proteins indicated several mitochondrial proteins (Appendix Fig S1B), consistent with interactors screens previously performed with OTULIN and HOIP (Kupka et al, 2016a; Stangl et al, 2019). Moreover, mitochondrial proteins were found in a study on proteome-wide dynamics of phosphorylation and ubiquitination in TNF-induced signaling (Wagner et al, 2016). These findings prompted us to explore a possible mitochondrial localization of OTULIN and HOIP. Mitochondria from

HEK293T cells were isolated and purified by subcellular fractionation using differential centrifugation followed by isopycnic density gradient centrifugation (Fig EV1A and B). Immunoblotting of purified mitochondrial fractions revealed that a small fraction of both OTULIN and HOIP co-purified with mitochondria (Fig 1A). We wondered whether OTULIN antagonizes M1-ubiquitination at mitochondria and therefore silenced OTULIN expression by RNA interference. Immunoblotting of mitochondrial fractions using the M1-ubiquitin-specific antibodies 1E3 or 1F11/3F5/Y102L (Matsumoto *et al*, 2012) revealed a strong M1-ubiquitin-positive signal at mitochondria isolated from OTULIN-silenced cells, indicating that OTULIN regulates mitochondrial M1-ubiquitination (Fig 1A and B). Based on the fact that TNF activates LUBAC (Haas *et al*, 2009; Rahighi *et al*, 2009; Tokunaga *et al*, 2009) and the identification of mitochondrial proteins in the proteome analysis of TNF signaling (Wagner *et al*, 2016), we were wondering whether TNF triggers linear ubiquitin chain formation at mitochondria. M1-linked ubiquitin chains were detected 15 min after TNF treatment at mitochondria isolated from various cell types, such as HEK293T, HeLa, SH-SY5Y cells, and mouse embryonic fibroblasts (MEFs) (Fig 1A–C). TNF-induced mitochondrial M1-ubiquitination was not observed in HOIP CRISPR/Cas9 knockout (KO) cells, confirming HOIP-dependent linear ubiquitination (Fig 1D). Co-localization of M1-linked ubiquitin with mitochondria after TNF treatment was also seen by immunocytochemistry followed by super-resolution structured illumination microscopy (SR-SIM) (Fig 1E). Consistent with an increase in mitochondrial M1-ubiquitination, the abundance of all three LUBAC components, HOIP, HOIL-1L, and SHARPIN, was increased at mitochondria after TNF treatment (Fig 1F). Immunoblotting of mitochondrial fractions showed that M1-ubiquitination at mitochondria is a fast and transient response with maximum intensity after 15 min, which is paralleled by an increase in K63-ubiquitination (Fig 1G). This is in line with the observation that linear ubiquitin chains are preferentially assembled as heterotypic K63/M1-linked chains (Emmerich *et al*, 2013, 2016; Fiil *et al*, 2013; Hrdinka *et al*, 2016; Cohen & Strickson, 2017).

### TNF stabilizes PINK1 at mitochondria

Next, we addressed the functional consequences of TNF-induced mitochondrial ubiquitination. Ubiquitination of mitochondrial outer membrane proteins has been linked to a mitochondrial quality

control pathway, resulting in the clearance of mitochondria by mitophagy (Nguyen *et al*, 2016; Whitworth & Pallanck, 2017; Harper *et al*, 2018; Pickles *et al*, 2018; Montava-Garriga & Ganley, 2020; Goodall *et al*, 2022). In this pathway, depolarization of the inner mitochondrial membrane leads to an import arrest and stabilization of the mitochondrial kinase PINK1 at the outer mitochondrial membrane. PINK1 is then activated by autophosphorylation and phosphorylates ubiquitin and the ubiquitin-like domain of the E3 ubiquitin ligase Parkin at serine 65, thereby activating Parkin (Gan *et al*, 2022; Kakade *et al*, 2022; Rasool *et al*, 2022; Sauve *et al*, 2022). Parkin-mediated ubiquitination of outer membrane proteins recruits the autophagic machinery to eliminate damaged mitochondria. When the mitochondrial membrane potential is intact, full-length PINK1 is imported by the translocases of the outer and inner mitochondrial membranes, the TOM and TIM23 complexes, and then PINK1 is processed to a 60 kDa intermediate species by the mitochondrial processing peptidase (MPP) in the matrix. Subsequently, the presenilin-associated rhomboid-like protein (PARL) and presumably other proteases in the inner membrane generate a 52-kDa mature PINK1 fragment (Fig EV1C and D) (Whitworth *et al*, 2008; Jin *et al*, 2010; Deas *et al*, 2011; Meissner *et al*, 2011; Shi *et al*, 2011; Greene *et al*, 2012). Proteolytically processed PINK1 is retro-translocated to the mitochondrial outer membrane, where it is ubiquitinated and rapidly degraded by the proteasome (Yamano & Youle, 2013; Liu *et al*, 2017). Whereas nonimported full-length PINK1 has been linked to mitophagy induction, little is known about the function of mature PINK1 and the conditions that increase its abundance.

The artificial tethering of unbranched linear ubiquitin chains to the mitochondrial outer membrane was shown to induce mitophagy (Yamano *et al*, 2020), we therefore tested whether mitochondrial M1-ubiquitination induced by TNF has an impact on mitophagy. We first compared the relative amounts of PINK1 species in untreated, TNF-stimulated, and CCCP (carbonyl cyanide 3-chlorophenylhydrazone)-treated cells. As expected, dissipation of the proton-motive force across the mitochondrial inner membrane by CCCP (10  $\mu$ M, 90 min) stabilized the unprocessed 63 kDa PINK1 species due to an impeded mitochondrial import. Upon 15 min TNF treatment, we observed a small but significant increase in PINK1 abundance (Fig 2A and B). Interestingly, M1-ubiquitination at mitochondria induced by TNF treatment or OTULIN silencing also increased the processed PINK1 species (Fig 2A). TNF-induced

#### Figure 1. TNF induces M1-linked ubiquitination at mitochondria.

- A, B A fraction of OTULIN is localized at mitochondria where it suppresses M1-linked ubiquitination. HEK293T cells were transfected with control or OTULIN siRNA. Cells were harvested 72 h (A) or 48 h (B) after transfection or 15 min after TNF treatment (25 ng/ml). Mitochondria were isolated by differential centrifugation and purified by ultracentrifugation using an OptiPrep™ density gradient. 38% (A) or 20% (B) of the mitochondrial fractions and 2% (A, B) of whole cell lysates were analyzed by immunoblotting using the antibodies indicated. For the detection of M1-linked ubiquitin chains, either the 1E3 (A) or the 1F11/3F5/Y102L (B) antibody was used.
- C TNF induces M1-ubiquitination at mitochondria in various cell types. The indicated cell types were treated with TNF (25 ng/ml, 15 min) and purified mitochondrial fractions analyzed as described in (A).
- D TNF-induced mitochondrial M1-ubiquitination does not occur in HOIP-deficient cells. Wildtype (WT) and HOIP-KO HAP cells were treated with TNF (25 ng/ml, 15 min) and analyzed as described in (A).
- E Mitochondria and M1-linked ubiquitin co-localize after TNF treatment. SH-SY5Y cells were treated with TNF (25 ng/ml, 15 min), fixed, stained with antibodies against HSP60 (green) and M1-ubiquitin (1E3, red), and analyzed by SR-SIM. Scale bar, 5  $\mu$ m.
- F TNF induces recruitment of LUBAC components to mitochondria. HEK293T cells were treated with TNF (25 ng/ml, 15 min) and analyzed as described in (A).
- G TNF induces a fast and transient increase in M1- and K63-specific ubiquitination at mitochondria. HEK 293T cells were treated with TNF (25 ng/ml) for the indicated time and the mitochondrial fractions were analyzed by immunoblotting using M1-, K63-, and K48-specific ubiquitin antibodies.

Source data are available online for this figure.

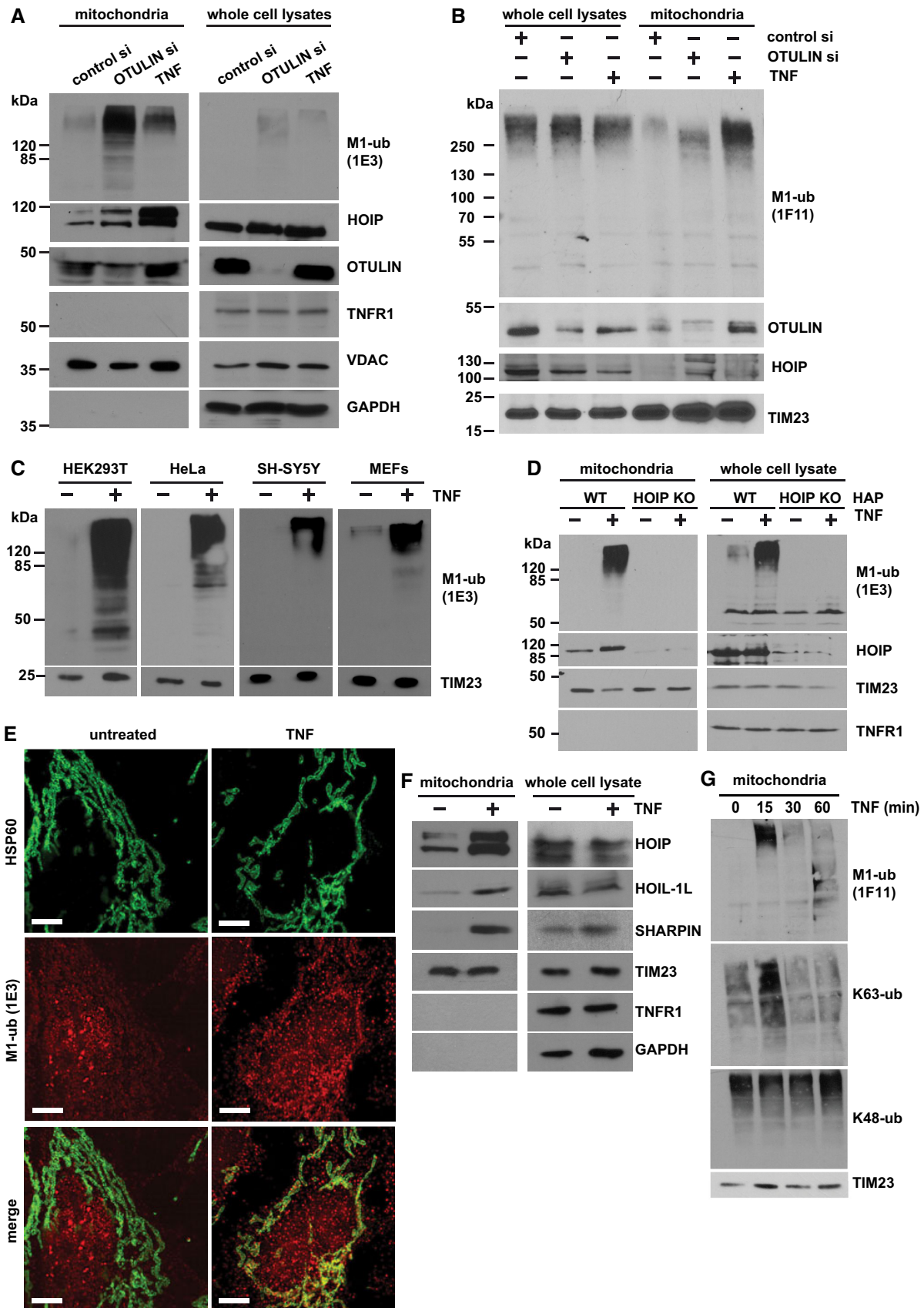


Figure 1.

PINK1 stabilization was accompanied by a slight increase in p-S65-ubiquitin and p-S65-Parkin signal intensities (Fig 2B).

A kinetic analysis of TMRE (tetramethylrhodamine ethyl ester) fluorescence in TNF-treated cells indicated a mild transient increase in the membrane potential between 15 and 60 min (Fig EV2A), revealing that PINK1 was not stabilized by dissipation of the mitochondrial membrane potential in TNF-treated cells. Consistent with this result, TNF-induced PINK1 stabilization at mitochondria did not induce mitophagy. Quantitative assessment of mitophagy by flow cytometry using the fluorescent reporter mt-mKeima did not reveal changes in mitophagic activity induced by TNF treatment up to 16 h (Figs 2C and EV2C). Moreover, mitophagy was not affected by OTULIN silencing or overexpression, suggesting that M1-linked ubiquitin chains do not regulate mitophagy (Fig EV2C–E), in line with proteomic ubiquitin profiling (Ordureau et al, 2014, 2018).

It has been reported previously that the mature 52-kDa PINK1 species is stabilized by K63-linked ubiquitination induced by NF- $\kappa$ B pathway activation (Lim et al, 2015). We therefore wondered whether PINK1 is a target for linear ubiquitination. Co-immunoprecipitation experiments indicated that PINK1 interacts with HOIP (Fig EV3A–D). To map the domains of HOIP mediating this interaction, we employed transiently transfected cells. V5-tagged PINK1 co-purified with full-length HOIP and the N-terminal part of HOIP (aa 1–697), but not with the C-terminal part of HOIP (aa 697–1,072) (Fig EV3A and B). We then tested different HOIP constructs lacking N-terminal domains to more precisely define the region of HOIP that mediates the interaction with PINK1. PINK1 co-immunoprecipitated only with the 1–697 aa HOIP construct and to a lesser extent with the 1–475 aa construct, which lacks the UBA domain, suggesting that the UBA domain directly or indirectly contributes to the interaction of HOIP with PINK1 (Fig EV3C and D). Of note, immunoblotting of cellular lysates indicated that PINK1 abundance was increased in the presence of either full-length HOIP or N-terminal HOIP (1–697 aa), suggesting that complex formation contributes to PINK1 stabilization (Fig EV3B and D, input). In support of PINK1 interacting with endogenous HOIP, both proteins were detected in the 450–720 kDa fractions (corresponding to the size of LUBAC) upon size-exclusion chromatography of cellular lysates

(Fig EV3E). In the next step, PINK1 ubiquitination was analyzed in cells overexpressing HOIP and HOIL-1 to increase LUBAC activity. The cells were harvested under denaturing conditions and then PINK1 was affinity-purified by its V5 tag and subjected to immunoblotting using ubiquitin antibodies. A strong ubiquitin-positive signal in the higher molecular range occurred upon increased expression of HOIP and HOIL-1, which was not present in cells overexpressing OTULIN, confirming a linear ubiquitin chain topology (Fig 2D). Compared with wildtype HOIP, only a weak ubiquitin-positive signal was seen in cells overexpressing catalytically inactive HOIP C885A (Fig 2D), which can be explained by the ability of co-expressed HOIL-1L to increase endogenous LUBAC activity. An *in vitro* ubiquitination assay using catalytically active recombinant HOIP and PINK1 immunoprecipitated from cells also supported the notion that HOIP can ubiquitinate PINK1 (Fig 2E). We then tested for ubiquitination of endogenous PINK1 after TNF treatment. PINK1 was immunoprecipitated from untreated or TNF-treated cells and analyzed by immunoblotting using PINK1-, M1-ubiquitin, and p-S65-ubiquitin-specific antibodies. Increased signal intensities were observed in the high molecular weight range in TNF-treated cells, which disappeared when the cell lysates were treated with recombinant OTULIN (Fig 2F). In conclusion, TNF signaling induces recruitment of LUBAC to mitochondria, where PINK1 is stabilized by complex formation and ubiquitination.

#### PINK1 counteracts OTULIN activity at mitochondria by phosphorylating M1-linked ubiquitin chains

What could be the functional consequence of PINK1 stabilization at the mitochondrial outer membrane? PINK1-mediated phosphorylation of ubiquitin alters the structure and surface properties of ubiquitin and thereby can affect the assembly and disassembly of polyubiquitin chains (Wauer et al, 2015). It has been shown previously *in vitro* that M1-linked tetra-ubiquitin is less efficiently hydrolyzed by OTULIN in the presence of PINK1 (Wauer et al, 2015). We confirmed these results (Fig EV3F and G) and tested whether PINK1 impairs OTULIN activity also in cells. Proteins modified by linear polyubiquitin chains were affinity-purified using the recombinant

#### Figure 2. PINK1 is stabilized at mitochondria by LUBAC-mediated ubiquitination.

- A, B PINK1 is stabilized by TNF treatment. HEK293T cells were treated with TNF (25 ng/ml, 15 min) or CCCP (10  $\mu$ M, 90 min) before harvesting or incubated with OTULIN-specific siRNA for 48 h (A). Purified mitochondrial fractions were analyzed by immunoblotting using the indicated antibodies. Quantification of PINK1-specific signals normalized to TIM23 is shown in the right panel. Data represent the mean values with standard deviations of four independent experiments. \* $P < 0.05$ . A two-tailed nonparametric Mann–Whitney *U*-test was used to analyze statistical significance. In (A), \*unprocessed PINK1; \*\*processed PINK1.
- C TNF-induced PINK1 stabilization does not induce mitophagy. HeLa cells expressing mt-mKeima were treated with TNF (25 ng/ml) for 30 min or 16 h. As a control, mt-mKeima -expressing HeLa cells were treated with antimycin A and oligomycin (A/O, 10  $\mu$ M each) for 1 h. The analysis was done by flow cytometry gating lysosomal and neutral mt-mKeima.
- D Catalytically active HOIP ubiquitinates overexpressed PINK1. HEK293T cells were transfected with the plasmids indicated. After 24 h, the cells were harvested under denaturing conditions and PINK1 was immunoprecipitated via the V5 tag followed by immunoblotting against ubiquitin.
- E Recombinant HOIP ubiquitinates PINK1 *in vitro*. V5-tagged-PINK1 immunoprecipitated from transiently transfected HEK293T cells via the V5 tag was incubated with recombinant mouse Ube1, UBE2L3, C-terminal HOIP, and ubiquitin for *in vitro* ubiquitination. The samples were then analyzed by immunoblotting using V5 antibodies.
- F Endogenous PINK1 is modified with M1-ubiquitin chains after TNF treatment. HEK293T cells were treated with TNF (25 ng/ml, 15 min), then endogenous PINK1 was immunoprecipitated from mitochondrial fractions. Cells mildly overexpressing PINK1-V5 were also included (lanes 4, 5, 8), to make sure that the immunoreactive bands seen for endogenous PINK1 indeed correspond to PINK1. As a control for the presence of M1-linked ubiquitin chains, immunoprecipitated PINK1 was treated with recombinant OTULIN. As controls for the specificity of the immunoprecipitation, beads only (lanes 6–8) and beads plus IgG (lane 9) were included. The samples were analyzed by immunoblotting using antibodies against PINK1, M1-ubiquitin, and phosphorylated ubiquitin. For immunoprecipitation of overexpressed PINK1, only 50% of cells were used in comparison to the immunoprecipitation of endogenous PINK1.

Source data are available online for this figure.

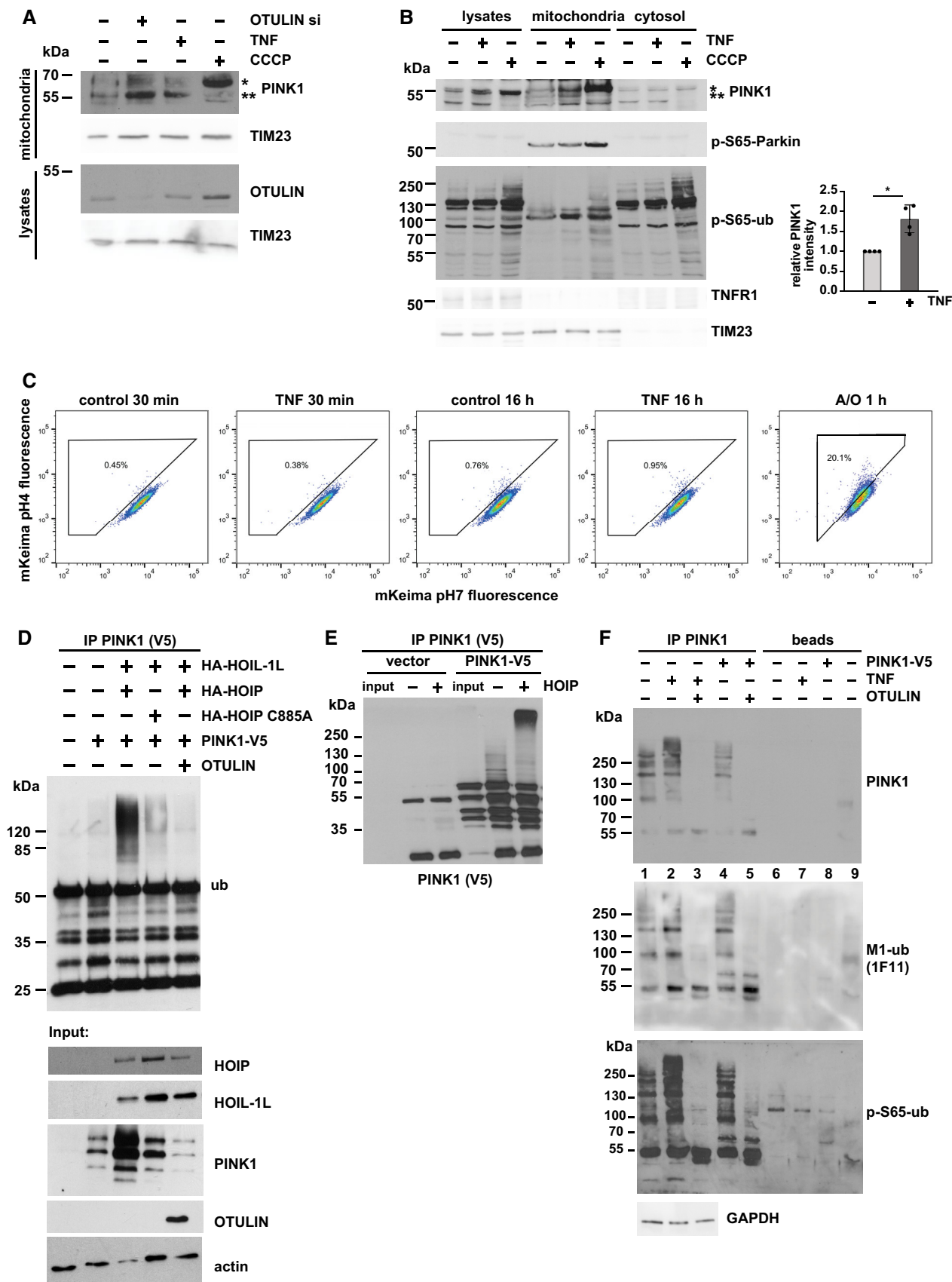


Figure 2.

UBAN domain of NEMO (Komander *et al*, 2009; Rahighi *et al*, 2009; Hadian *et al*, 2011; Muller-Rischart *et al*, 2013), which shows a 100-fold higher affinity for M1-linked than for K63-linked ubiquitin (Lo *et al*, 2009; Rahighi *et al*, 2009), and then analyzed by immunoblotting using M1-ubiquitin-specific antibodies. The M1-ubiquitin-positive signals in extracts prepared from cells overexpressing HOIP and HOIL-1L were abolished by co-expression of wildtype OTULIN (Fig 3A, lanes 1 and 4) but not by the inactive OTULIN variant W96A (Fig 3A, lane 6). Co-expression of PINK1 increased M1-ubiquitination induced by HOIP and HOIL-1L (Fig 3A, lanes 1 and 2) and partially restored M1-ubiquitination in cells co-expressing wildtype OTULIN (Fig 3A, lanes 3 and 4). These results suggested that also in cells PINK1 can counteract the efficiency of OTULIN to hydrolyze M1-linked polyubiquitin chains.

Prompted by these findings, we wondered whether PINK1 increases TNF-induced M1-ubiquitination at mitochondria by phosphorylating ubiquitin. Increased expression of wildtype PINK1 but not kinase-dead (K/D) PINK1 increased p-S65-ubiquitin in the mitochondrial fraction after TNF treatment (Fig 3B), whereas in cells silenced for PINK1 expression TNF did not increase p-S65-ubiquitin (Fig 3C). In favor of a role of PINK1 in stabilizing M1-linked ubiquitin chains, the TNF-induced M1-ubiquitin-specific signal was significantly reduced in MEFs from PINK1-KO mice (Fig 3D).

### Mitochondrial M1-ubiquitination protects from apoptosis

Our data so far revealed that TNF increases M1-linked ubiquitination at mitochondria and stabilizes PINK1 without inducing mitophagy. Based on the fact that both TNF and PINK1 have anti-apoptotic functions, we were wondering whether M1-ubiquitination at mitochondria protects from cell death. TNF induces the increased expression of anti-apoptotic proteins through the formation of complex I at the TNFR1 and activation of the transcription factor NF- $\kappa$ B (Hayden & Ghosh, 2014; Brenner *et al*, 2015; Kupka *et al*, 2016b). We hypothesized that the fast TNF-induced increase in mitochondrial ubiquitination protects mitochondria from apoptosis before transcriptional reprogramming by NF- $\kappa$ B takes effect. To address this possibility experimentally, we exposed cells to a short proapoptotic stimulus with or without TNF pretreatment for 15 min. Apoptotic cell death was assessed by mitochondrial Bax recruitment, cytochrome *c* release, caspase-3 activation, and ultrastructural

analysis of cristae morphology. Bax was efficiently recruited to mitochondria within 1 h of staurosporine (STS) treatment, as detected by immunoblotting of purified mitochondria (Fig 4A). When STS was applied 15 min after TNF pretreatment, the amount of mitochondrial Bax was significantly reduced (Fig 4A). Likewise, STS-induced cytochrome *c* release into the cytoplasm was decreased by the TNF pretreatment (Fig 4B). Electron microscopy revealed that TNF prevents the STS-induced reduction in cristae abundance per mitochondrial area and cristae length per mitochondria (Fig 4C and D). Moreover, TNF significantly reduced the number of STS-treated cells with activated caspase-3 (Fig 4E). This effect was not compromised in the presence of the NF- $\kappa$ B super-repressor I $\kappa$ B $\alpha$  (serines 32 and 36 replaced by alanines), which blocks nuclear translocation of the NF- $\kappa$ B subunit p65 and thus NF- $\kappa$ B transcriptional activity (Sun *et al*, 1996; Appendix Fig S2A and B), indicating that the fast protective effect of TNF was not mediated by NF- $\kappa$ B activation (Fig 4E). Notably, both HOIP and PINK1 were required for the protective effect of TNF pretreatment, since in cells silenced for HOIP or PINK1 expression, TNF was not able to reduce STS-induced cytochrome *c* release (Fig 4F and G). We concluded that the TNF-induced assembly of M1-linked ubiquitin chains by HOIP and their phosphorylation by PINK1 interferes with the insertion of Bax into the outer mitochondrial membrane, thereby preventing apoptotic cell death. To check for mitochondrial fitness, we also analyzed cellular bioenergetics in response to TNF treatment and observed a transient increase in maximal respiration, spare respiratory capacity, and ATP production (Fig EV4A–C), suggesting that TNF at least transiently enhances the cellular energy metabolism.

### A signaling platform for TNF-induced NF- $\kappa$ B activation is assembled at mitochondria

Why is mitochondrial fitness and protection fostered in the early phases of TNF signaling? Though the fast TNF-mediated protection of mitochondria from apoptosis was NF- $\kappa$ B-independent, we observed an increased abundance of NEMO, p65, and phosphorylated p65 (p65) at mitochondria after 15 min TNF treatment (Fig 5A). We therefore speculated that mitochondrial M1-ubiquitination contributes to TNF signal amplification and facilitates transmission of the signal to the nucleus. To confirm our data based on mitochondrial purification and immunoblotting, we performed a

**Figure 3. PINK1 stabilizes M1-linked ubiquitin by phosphorylation and counteracts OTULIN activity.**

- PINK1 antagonizes OTULIN activity in cells. HEK293T cells expressing HOIP and HOIL-1L were transfected with PINK1, WT OTULIN, or the inactive OTULIN mutant W96A, as indicated. The cells were lysed 24 h later under denaturing conditions, and lysates were subjected to affinity purification using the Strep-tagged UBAN domain of NEMO to enrich proteins modified with M1-linked ubiquitin. Proteins affinity-purified by Strep-Tactin beads were immunoblotted against ubiquitin.
- Catalytically active PINK1 increases p-S65-ubiquitin at mitochondria. HEK293T cells were transfected with wildtype PINK1 or kinase-dead (K/D) PINK1. Forty-eight hours after transfection, the cells were treated with TNF (25 ng/ml, 15 min) and lysed. Purified mitochondrial fractions were analyzed by immunoblotting using antibodies against p-S65-ubiquitin, PINK1, and VDAC (loading control).
- The TNF-induced increase in p-S65-ubiquitin is abolished in PINK1-deficient cells. HEK293T cells were transfected with control or PINK1-specific siRNA and treated with TNF (25 ng/ml, 15 min) or CCCP (10  $\mu$ M, 90 min) 48 h after transfection. The whole cell lysates were analyzed by immunoblotting using the indicated antibodies.
- TNF-induced M1-ubiquitination is reduced in PINK1-deficient cells. WT and PINK1-KO MEFs were treated with TNF (25 ng/ml, 15 min) and then harvested. Purified mitochondrial fractions were subjected to affinity purification using the Strep-tagged UBAN domain, as described in (A), followed by immunoblotting using M1-ubiquitin-specific antibodies, Strep-Tactin conjugated to horse radish peroxidase (to control the UBAN pulldown efficiency), and TIM23 (input control). Quantification of the M1-ubiquitin-positive signal intensities is shown in the lower panel. Data represent the mean values with standard deviations of three independent experiments; n.s., not significant, \*\*\* $P$  < 0.001. A two-way ANOVA test was used to analyze statistical significance.

Source data are available online for this figure.

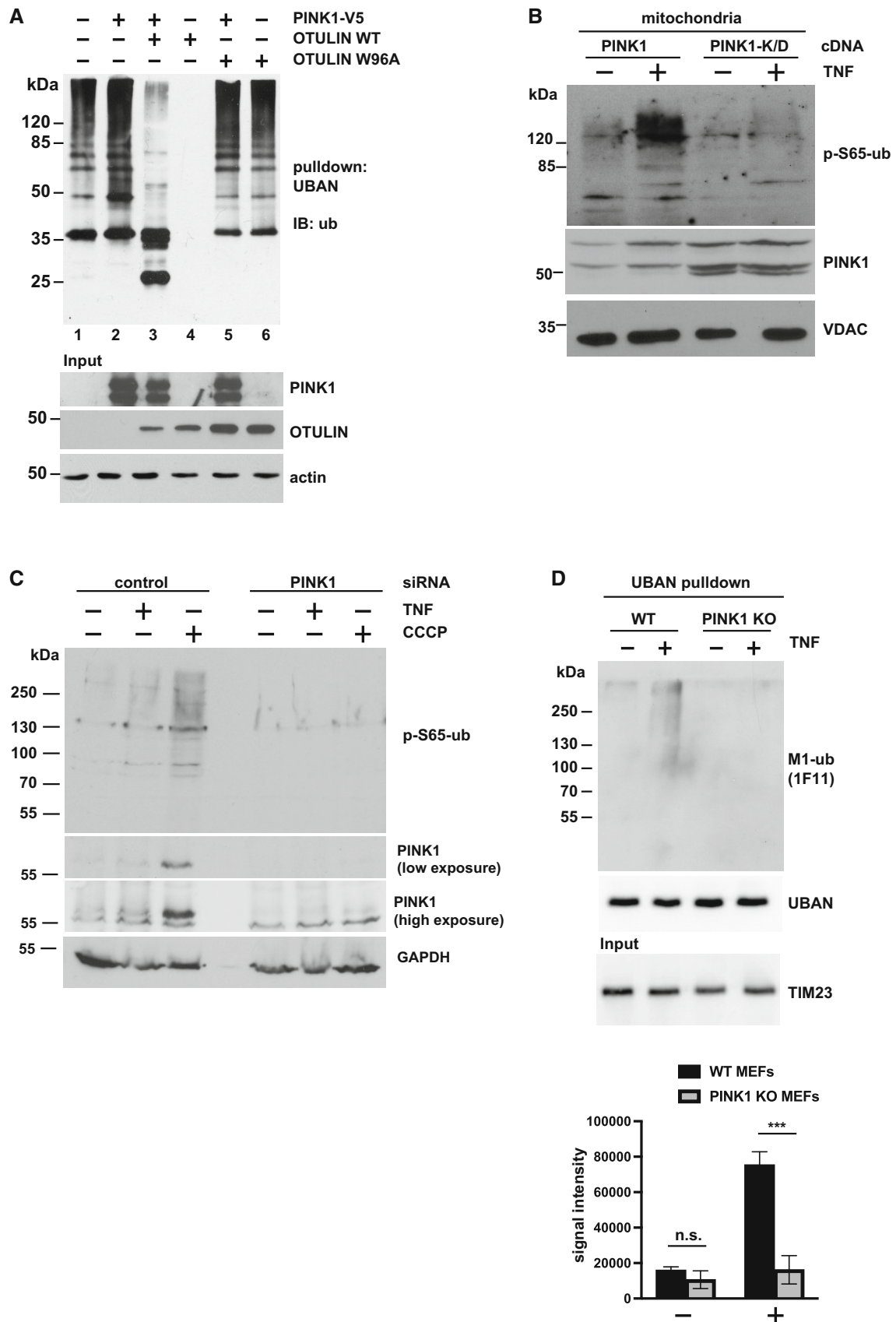


Figure 3.



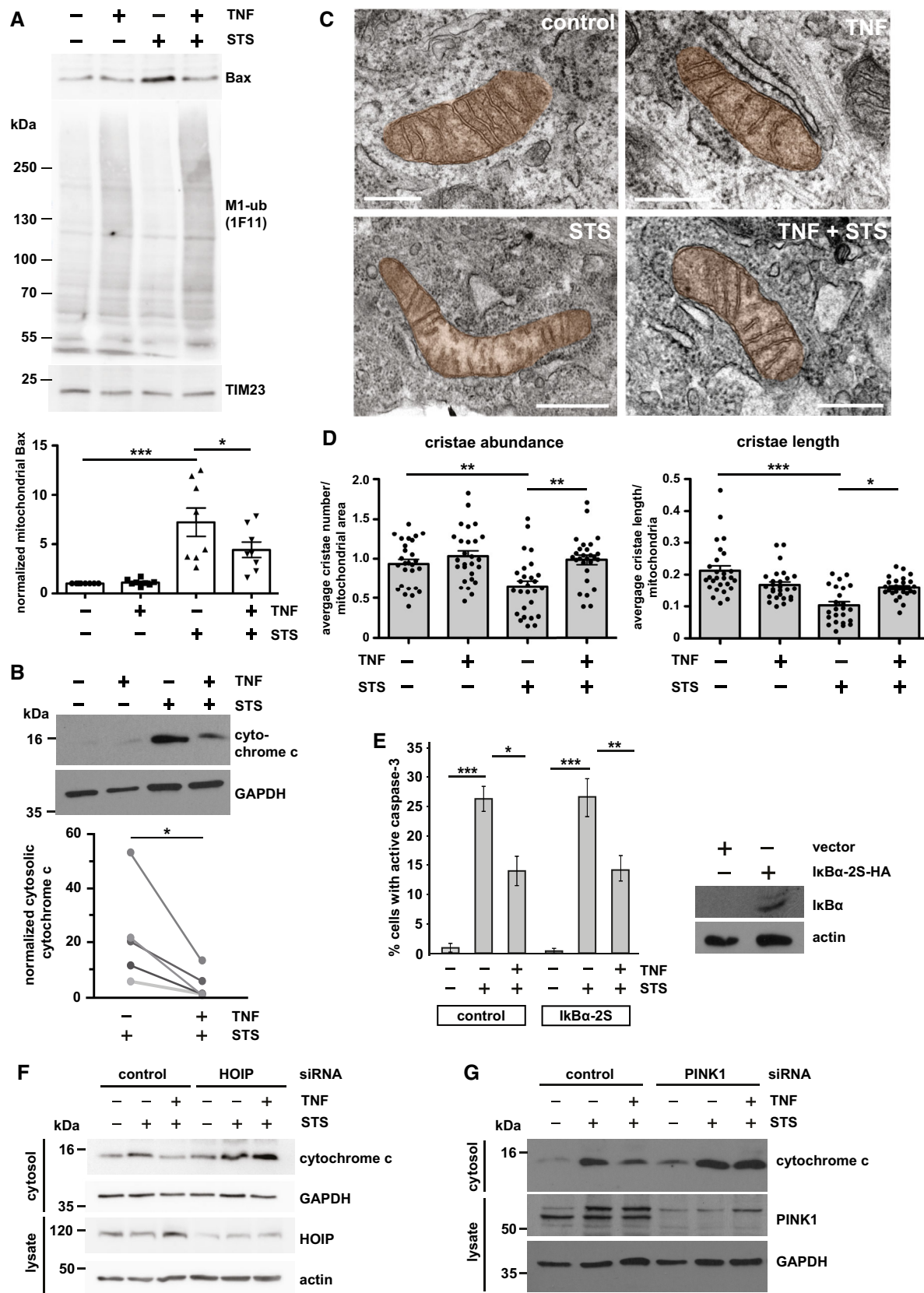


Figure 4.

**Figure 4. M1-ubiquitination at mitochondria protects from apoptosis.**

- A STS-induced mitochondrial Bax recruitment is reduced by TNF. HeLa cells were treated with STS (1  $\mu$ M, 1 h) with or without a 15 min pretreatment with TNF (25 ng/ml) and then harvested. Purified mitochondrial fractions were analyzed by immunoblotting using antibodies against Bax and M1-ubiquitin. The input was immunoblotted for TIM23 (upper panel). Bax-specific signal intensities were quantified and normalized to TIM23-specific signals (lower panel). Data represent the mean with standard error of eight independent experiments. \* $P < 0.05$ , \*\*\* $P < 0.001$ . Kruskal–Wallis test followed by Dunn's multiple comparison test,  $n = 8$ .
- B STS-induced cytochrome c release is decreased by TNF. HeLa cells were treated as described in (A). The cytosolic fractions were analyzed by immunoblotting using cytochrome c antibodies. GAPDH was used as a reference. Quantification of five biological replicates is shown in the lower panel. Signal intensities were quantified and normalized to that of GAPDH. \* $P < 0.05$ . Kolmogorow–Smirnov normality test, paired  $t$ -test, two-tailed,  $n = 5$ .
- C, D TNF treatment prevents damage of mitochondrial cristae under proapoptotic conditions. (C) SH-SY5Y cells were treated as described in (A), fixed and embedded and the mitochondrial ultrastructure was imaged by electron microscopy. Scale bar: 400 nm. (D) Cristae abundance (average cristae number per mitochondrial area) and cristae length (average cristae length per mitochondrion) were analyzed by Imaris 9.8. \* $P < 0.05$ , \*\* $P < 0.01$ , \*\*\* $P < 0.001$ . Cristae abundance: Shapiro–Wilk normality test, One-way ANOVA followed by Tukey's multiple comparison test,  $n = 27$ . Cristae length: Kruskal–Wallis test followed by Dunn's multiple comparison test,  $n = 24–27$ . Bars represent mean  $\pm$  SEM.
- E The fast anti-apoptotic effect of TNF is not affected by the NF- $\kappa$ B inhibitor I $\kappa$ B $\alpha$ . SH-SY5Y cells were transiently transfected with the NF- $\kappa$ B super-repressor I $\kappa$ B $\alpha$ -2S or luciferase as a control. Twenty-four hours later, the cells were treated with STS (5  $\mu$ M, 2 h) with or without a 15 min pretreatment with TNF (25 ng/ml). Cells were fixed and stained by antibodies against active caspase-3. Signal intensities were quantified by immunocytochemistry and I $\kappa$ B $\alpha$ -2S was tested by immunoblotting using antibodies against the HA tag. Data represent the standard deviation of three independent experiments; at least 300 cells were counted per experiment. \* $P < 0.05$ , \*\* $P < 0.01$ . Student's  $t$ -test, two-tailed,  $n = 3$ .
- F The protective effect of TNF is dependent on HOIP expression. HeLa cells were transiently transfected with control or HOIP siRNA. Forty-eight hours after transfection, cells were treated with STS (1  $\mu$ M, 1 h) with or without a 15 min TNF pretreatment (25 ng/ml) and then harvested. The cytosolic fractions were analyzed by immunoblotting using cytochrome c antibodies. HOIP silencing efficiency was analyzed in whole cell lysates using antibodies against HOIP. GAPDH and actin were immunoblotted as input controls.
- G The protective effect of TNF is dependent on PINK1 expression. HeLa cells were transiently transfected with control or PINK1 siRNA and treated as described in (F). The cytosolic fractions were analyzed by immunoblotting using cytochrome c and PINK1 antibodies. GAPDH was immunoblotted as input control.

Source data are available online for this figure.

proximity ligation assay (PLA). *In situ* PLA using anti-TOM20 and anti-phospho-S536-p65 (p-p65) antibodies revealed the presence of p-p65 at mitochondria and an increased abundance upon TNF treatment (Fig 5B and C).

Next, we tested whether PINK1 has a role in mitochondrial NF- $\kappa$ B pathway activation. TNF-induced nuclear translocation of p65 was significantly decreased in cells silenced for PINK1 expression. This phenotype was rescued by wildtype PINK1 but not by the catalytically inactive PINK1-K/D mutant (Fig 6A). Moreover, luciferase reporter assays indicated that basal and TNF-induced NF- $\kappa$ B-dependent transcription is reduced in cells silenced for PINK1 expression (Fig EV4D), in line with earlier findings (Sha *et al*, 2010). NEMO is a highly relevant substrate of HOIP in NF- $\kappa$ B pathway activation, and we and others previously found that Parkin modifies NEMO with K63-linked ubiquitin chains (Henn *et al*, 2007; Sha *et al*, 2010; Van Humbeek *et al*, 2011; Muller-Rischart *et al*, 2013). We therefore explored the possibility that PINK1 phosphorylates ubiquitinated NEMO. In cells expressing wildtype PINK1, the p-S65-ubiquitin signal was strongly enhanced on NEMO affinity-purified from cell lysates, whereas no signal was seen when catalytically inactive PINK1-K/D was expressed

(Fig 6B). Supporting the physiological relevance of endogenous PINK1, TNF-induced M1-ubiquitination of NEMO was reduced in PINK1-deficient cells (Fig 6C). Taken together, catalytically active PINK1 promotes NF- $\kappa$ B activation, most likely by stabilizing M1-linked ubiquitin chains on LUBAC substrates, such as NEMO, through phosphorylation.

**TNF promotes transport of p65 to the nucleus and increases mitochondria-nucleus contact sites**

What could be the advantage of assembling a signaling platform at mitochondria? First, the mitochondrial network provides a large surface area for signal amplification. Second and possibly even more relevant, mitochondria are highly dynamic and mobile organelles that engage in physical and functional interactions with other organelles and the plasma membrane (Scorrano *et al*, 2019; Giacomello *et al*, 2020; Harper *et al*, 2020; Prinz *et al*, 2020). We therefore wondered whether mitochondria facilitate the transport of activated NF- $\kappa$ B components to the nucleus. First, we followed up on the motility of mitochondria in SH-SY5Y cells upon TNF stimulation by live cell imaging and observed a decrease in the distance between peripheral

**Figure 5. Mitochondria serve as a signaling platform for TNF-induced NF- $\kappa$ B activation.**

- A NF- $\kappa$ B signaling components are recruited to mitochondria upon TNF treatment. (A) HEK293T cells were treated with TNF (25 ng/ml, 15 min), harvested and purified mitochondrial fractions were analyzed by immunoblotting using the antibodies indicated; p-p65: phospho-S536-p65; p-TBK1: phospho-S172-TBK1.
- B Phosphorylated p65 is in close proximity to TOM20 in response to TNF treatment. Representative immunofluorescence images of SH-SY5Y cells using the proximity ligation assay (PLA) between phospho-S536-p65 (rabbit) and TOM20 (mouse) coupled antibodies. One set of cells was treated with TNF (25 ng/ml, 15 min) before fixation. Nuclei were stained with DAPI, mitochondria were stained with MitoTracker™ Red CMXRos (red), and the PLA amplification reaction was visualized by green foci. As a positive control, fixed cells were incubated with primary TOM20 (mouse) and TOM70 (rabbit) antibodies and subjected to the PLA assay. As negative controls, fixed cells were incubated with either TOM20 or p-p65 antibodies prior to the PLA assay. Scale bar, 10  $\mu$ m.
- C Quantification of the phospho-S536-p65/TOM20 PLA foci per cell. Data represent the number of PLA foci per cell (mean  $\pm$  SD); at least 84 cells in total were analyzed per condition. \*\*\*\* $P < 0.0001$ . A two-tailed nonparametric Mann–Whitney test was used to analyze statistical significance.

Source data are available online for this figure.

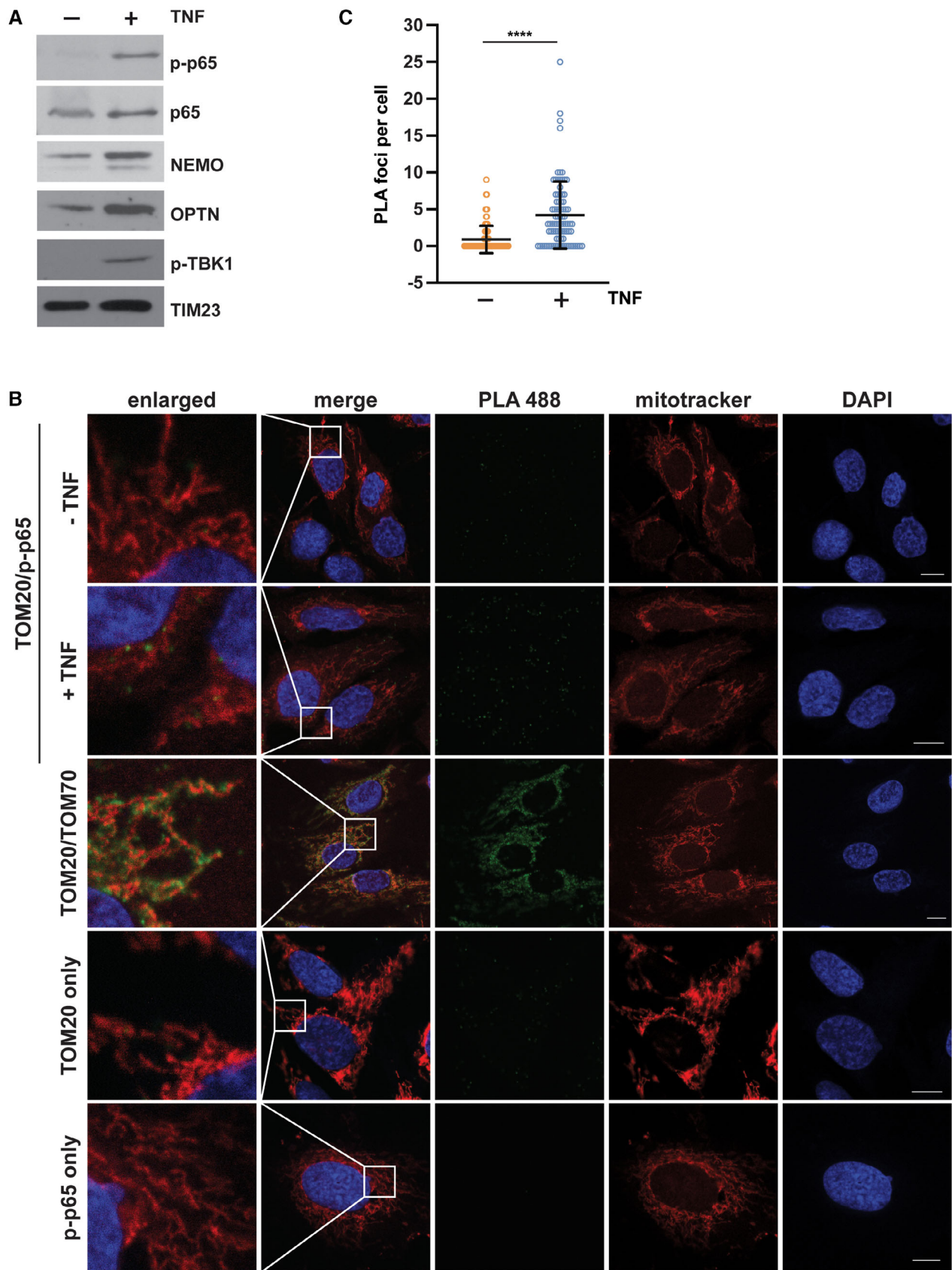


Figure 5.

mitochondria and the nucleus within 15 min of TNF treatment (Fig 7A; Movie EV1). Encouraged by this observation, we tested whether mitochondrial motility affects the nuclear translocation of p65 upon TNF stimulation. We silenced the expression of the mitochondrial outer membrane Rho GTPases Miro1 and Miro2, which are components of the adaptor complex that anchors mitochondria to motor proteins (Schwarz, 2013; Misgeld & Schwarz, 2017). A ratiometric analysis revealed a significant decrease in the fraction of nuclear p65 upon TNF stimulation in Miro1/2-deficient cells (Fig 7B). Accordingly, NF- $\kappa$ B-dependent transcription was decreased

in cells silenced for Miro1 and Miro 2 expression (Fig EV4E). We then reasoned that mitochondrial transport of p65 to the nucleus should increase the proximity between mitochondria and the nucleus and possibly favor the formation of mitochondria-nucleus contact sites. To this end, we have generated a new genetically encoded split-GFP contact site sensor (SPLICS) (Cieri et al, 2018; Vallese et al, 2020; Cali & Brini, 2021), capable to reconstitute fluorescence only when the nucleus and mitochondria are in close proximity (Fig 7C). Correct targeting and self-complementation ability of the GFP<sub>1-10</sub> and the  $\beta$ 11 split-GFP fragments to the outer nuclear

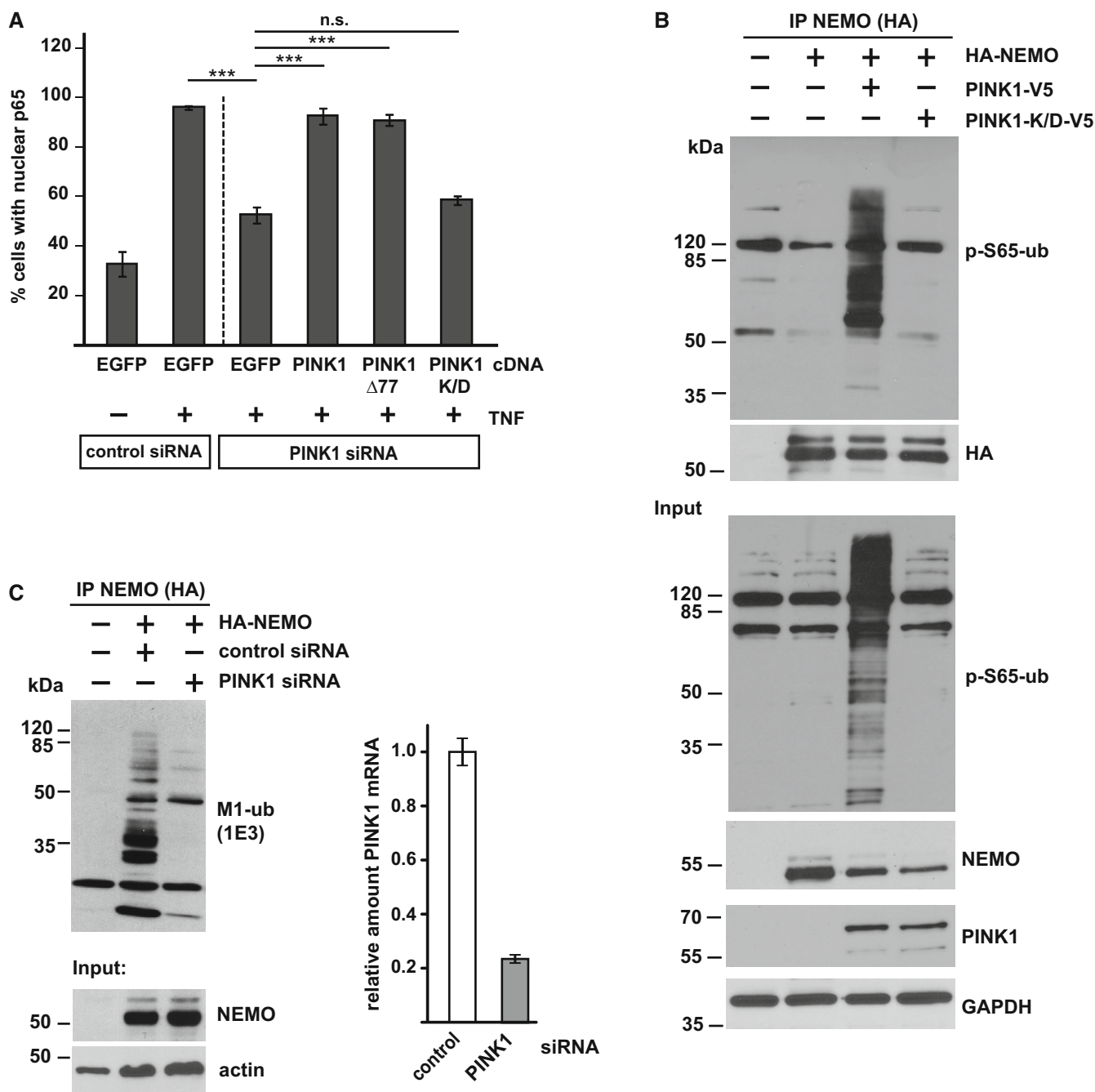


Figure 6.

**Figure 6. PINK1 promotes NF- $\kappa$ B activation and modulates NEMO ubiquitination.**

- A Nuclear translocation of p65 is impaired in cells silenced for PINK1 expression. SH-SY5Y cells were transfected with control or PINK1-specific siRNAs. For rescue experiments, cells were co-transfected with wildtype PINK1, PINK1 $\Delta$ 77, or kinase-dead PINK1-K/D. Two days after transfection the cells were treated with TNF (25 ng/ml, 25 min), fixed, and stained with p65 antibodies. The fraction of cells showing nuclear translocation of p65 was determined for each condition. Data represent the mean  $\pm$  SEM of three independent experiments. The experiment was performed in triplicates and more than 300 cells were quantified per experiment and condition. \*\*\* $P$  < 0.001, Student's  $t$ -test, two-tailed,  $n$  = 3.
- B PINK1 phosphorylates ubiquitinated NEMO. HEK293T cells were co-transfected with V5-tagged wildtype PINK1 or kinase-dead PINK1-K/D and HA-tagged NEMO. One day after transfection the cells were lysed and subjected to immunoprecipitation using antibodies against HA. Precipitated proteins were then detected by immunoblotting using p-S65-ubiquitin antibodies. The input was immunoblotted for NEMO, PINK1, p-S65-ubiquitin, and GAPDH.
- C Linear ubiquitination of NEMO is reduced in PINK1-deficient cells. HEK293T cells were co-transfected with HA-NEMO and control or PINK1-specific siRNAs. Forty-eight hours after transfection the cells were lysed and subjected to immunoprecipitation using antibodies against HA. Precipitated proteins were then detected by immunoblotting using M1-ubiquitin antibodies. The input was immunoblotted for NEMO and actin. PINK1 silencing efficiency was determined by real-time RT-PCR. Bars represent mean  $\pm$  SD with three technical replicates.

Source data are available online for this figure.

membrane (ONM) were tested (Fig EV5A–C). The ONM- $\beta$ 11 was further selected to generate the SPLICS<sup>NU-MT</sup> reporter along with the outer mitochondrial membrane (OMM)-targeted GFP<sub>1-10</sub>, which has been extensively used in all mitochondrial sensors generated so far (Fig 7D; Cieri *et al*, 2018; Vallese *et al*, 2020). Expression of the SPLICS<sup>NU-MT</sup> reporter in HeLa cells resulted in the emission of a fluorescent punctate signal within the nuclear/perinuclear region that could be easily quantified with the Fiji (<https://imagej.net/software/fiji/>) software, and custom macros written for interorganellar contact analysis (Cali & Brini, 2021), with an additional ROI traced around the nucleus of SPLICS<sup>NU-MT</sup>-positive cells to specifically focus only contacts that involve the nuclear envelope (Fig EV5D). To validate the ability of the SPLICS<sup>NU-MT</sup> reporter to detect changes in the mitochondria-nucleus contact sites, we triggered the mitochondrial retrograde response (MRR) in HeLa cells (Amuthan *et al*, 2001; Eisenberg-Bord & Schuldiner, 2017; Desai *et al*, 2020; Walker & Moraes, 2022). A significant increase in the formation of nucleus-mitochondria contact sites upon MRR activation was observed by employing the SPLICS<sup>NU-MT</sup> reporter (Fig EV5E). With this new tool, we assessed whether mitochondrial

transport of p65 to the nucleus favors the proximity between mitochondria and the nucleus in TNF-treated SPLICS<sup>NU-MT</sup>-expressing cells. Indeed, the number of mitochondria-nucleus contact sites strongly increased upon TNF stimulation (Fig 7E–G). Remarkably, HOIP silencing by siRNA completely abolished the TNF-induced increase in mitochondria-nucleus contacts (Fig 7H–J). Thus, different experimental approaches supported the notion that mitochondria are implicated in targeting activated NF- $\kappa$ B to the nucleus upon TNF stimulation and that this process is dependent on linear ubiquitination.

## Discussion

We identified a mitochondrial signaling platform for NF- $\kappa$ B pathway activation that is shaped by LUBAC-mediated linear ubiquitination. This mitochondrial platform shares some features with a signaling platform that is assembled at cytosol-invading bacteria, such as *Salmonella* species, to restrict bacterial proliferation. Ubiquitination of the bacterial outer membrane component lipopolysaccharide

**Figure 7. Mitochondria facilitate the transfer of p65 to the nucleus.**

- A TNF induces the movement of peripheral mitochondria toward the nucleus. Primary macrophages were stained by Mitotracker<sup>TM</sup> Green to visualize mitochondria and by Hoechst 33342 to visualize the nucleus and monitored every 30 s for 15 min after treatment with TNF (25 ng/ml). The motility of mitochondria was analyzed using Imaris 9.8 spot function. The graphical representation of the top 25% peripheral mitochondrial indicates a decrease in the average mitochondrial distance to the nucleus after TNF treatment. Exemplified dataset shows the median distance with the upper and lower quartile (shaded area) of  $n$  = 105–187 mitochondrial spots per time point.
- B Nuclear p65 translocation upon TNF treatment is reduced in cells silenced for Miro1/2 expression. HeLa cells were transfected with control or Miro1 and Miro2 siRNAs. 48 h later, cells were treated with TNF (25 ng/ml, 15 min), fixed, and stained using antibodies against p65 and tubulin and DAPI. Images were segmented in a cytoplasmic and nuclear compartment and the fluorescence signal intensity ratio of p65 was measured using CellProfiler 4.2.1. Quantification is based on three biological replicates. Kruskal–Wallis test followed by Dunn's multiple comparison test,  $n$  = 79–157, \* $P$  < 0.05.
- C Cartoon of newly developed SPLICS reporter to detect mitochondria-nucleus contact sites. Fluorescence reconstitution between the ONM-targeted  $\beta$ 11 and the OMM-targeted GFP<sub>1-10</sub> fragment occurs at the contact site.
- D Scheme of the plasmids encoding the SPLICS<sup>NU-MT</sup> reporter.
- E–G TNF increases mitochondria-nucleus contact sites. Representative immunofluorescence images (E, F) and quantification (G) of mitochondria-nucleus contact sites in HeLa cells transfected with the SPLICS<sup>NU-MT</sup> and treated with 25 ng/ml TNF or PBS for 15 min. TOM20 antibodies were used to stain mitochondria and p65 antibodies to assess p65 nuclear translocation. Nuclei were stained with Hoechst33342 (ThermoFisher, 1  $\mu$ g/ml). Unpaired two-tailed  $t$ -test,  $n$  = 43 (control) or 51 (TNF), Bars represent mean  $\pm$  SEM. \*\*\*\* $P$  < 0.0001. Scale bar: 10  $\mu$ m.
- H–J TNF increases mitochondria-nucleus contact sites in a HOIP-dependent manner. Representative immunofluorescence images (H, I) and quantification (J) of mitochondria-nucleus contact sites in control or HOIP-silenced (HOIP siRNA) HeLa cells transfected with the SPLICS<sup>NU-MT</sup> probe treated with 25 ng/ml TNF or PBS for 15 min. Mitochondria and nuclei were stained as described in (E) and (F). Two-way ANOVA followed by Tukey's multiple comparison test,  $n$  = 34–44 from three independent experiments, Bar represents mean  $\pm$  SEM. \*\*\*\* $P$  < 0.0001. Scale bar: 10  $\mu$ m.

Source data are available online for this figure.

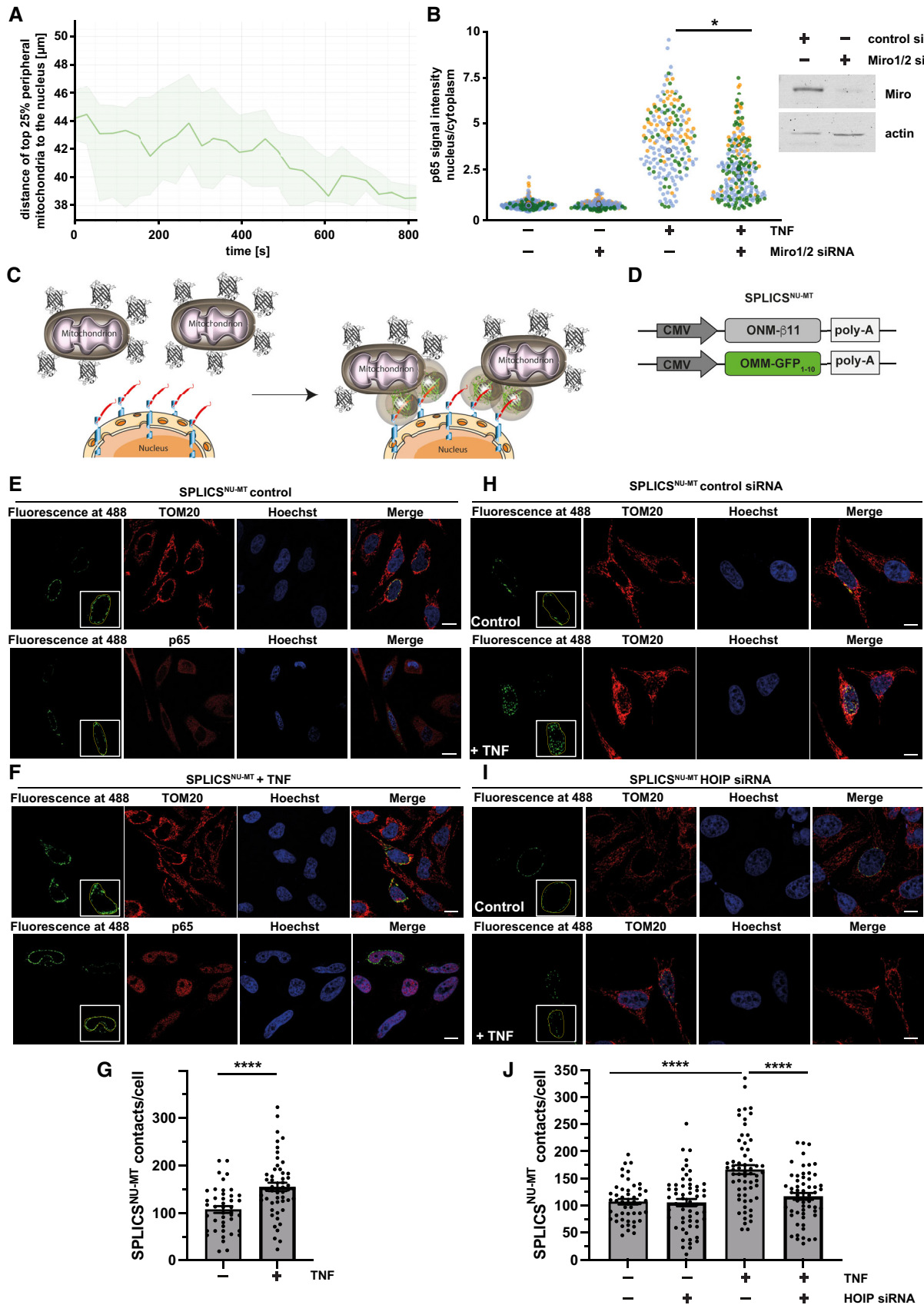


Figure 7.

(LPS) by the RNF213 ubiquitin ligase and subsequent binding of LUBAC to pre-existing ubiquitin results in the assembly of M1-linked ubiquitin chains and the recruitment of the M1-ubiquitin-binding proteins NEMO and Optineurin to the bacterial surface (Noad *et al*, 2017; van Wijk *et al*, 2017; Otten *et al*, 2021). NEMO induces local activation of NF- $\kappa$ B signaling, whereas Optineurin as a selective autophagy receptor promotes the autophagic clearance of bacteria. Similarly to the bacterial NF- $\kappa$ B signaling platform, we observed recruitment of LUBAC, formation of OTULIN-sensitive M1-linked ubiquitin chains, and binding and activation of NF- $\kappa$ B signaling components at the outer mitochondrial membrane. In contrast to the bacterial ubiquitin coat, enrichment of linear ubiquitin chains at mitochondria does not induce their autophagic clearance.

The formation of mitochondrial signaling platforms has been implicated in various signaling paradigms. However, many aspects of why cells employ mitochondria as signaling organelles are still unknown. One obvious advantage is that the integration of mitochondria in signaling pathways facilitates context-dependent adaptive responses to bioenergetic or biosynthetic demands. Another plausible explanation is that several signaling pathways affect cell fate decisions, which are regulated by mitochondria. Our study revealed two other advantages of mitochondrial signaling platforms. Mitochondria can contribute to signal amplification by virtue of their large surface and the presence of signaling components that stabilize “signals” by forming protein complexes (signalosomes) and/or by posttranslational modifications of signaling components. In TNF signaling, the mitochondrial kinase PINK1 performs such a function. It increases the stability of M1-linked ubiquitin chains assembled by HOIP by antagonizing the M1-ubiquitin-specific deubiquitinase OTULIN, thus enhancing downstream signaling. Moreover, mitochondria are highly dynamic and mobile organelles, allowing them to communicate and interact with various cellular components and organelles. Here we present evidence that mitochondria can act as vehicles to shuttle activated transcription factors to the nucleus. This mode of transport may be particularly relevant to polarized cells, such as neurons. In support of this notion, NF- $\kappa$ B signaling components are present at synapses and concentrated at postsynaptic densities together with mitochondria, where neuronal activity-dependent retrograde transport of the NF- $\kappa$ B subunit p65 serves as a synapse-to-nucleus signal transducer (Mikenberg *et al*, 2007; Shrum *et al*, 2009). In our study, nuclear translocation of the NF- $\kappa$ B subunit p65 upon TNF stimulation was decreased in cells silenced for Miro1 and Miro2 expression. Even more striking, we found that TNF increases mitochondria-nucleus contact sites, which presumably facilitate the uptake of p65 into the nuclear compartment. In support of this notion, the expression level of a mitochondria-nucleus tether component identified in breast cancer cells, the mitochondrial translocator protein TSPO, correlated with the abundance of nuclear NF- $\kappa$ B (Desai *et al*, 2020). TNF-induced formation of mitochondria-nucleus contact sites was dependent on HOIP, confirming a role of M1-linked ubiquitination. In a recent study performed in *Saccharomyces cerevisiae*, TOM70 has been implicated in the formation of tethers between mitochondria and the nucleus (Eisenberg-Bord

*et al*, 2021). TOM70 has also been identified as a target for ubiquitination within the TNF signaling network (Wagner *et al*, 2016) and was detected as an OTULIN-interacting protein in our mass spectrometry-based screen. In addition, TOM70 is required for the activation of IRF3 in MAVS signaling (Liu *et al*, 2010; Thorne *et al*, 2022). Hence, it will be interesting to explore the possible role of TOM70 in the NF- $\kappa$ B pathway.

TNF signaling usually mounts an anti-apoptotic response via the TNFR1/complex I/NF- $\kappa$ B axis, implicating transcriptional regulation of anti- and proapoptotic gene expression (Varfolomeev & Vucic, 2018). We previously identified the mitochondrial GTPase OPA1 as an NF- $\kappa$ B target gene, which contributes to anti-apoptotic reprogramming by maintaining cristae integrity (Muller-Rischart *et al*, 2013). Here we identified a fast, transcription-independent anti-apoptotic TNF response that protects mitochondria by remodeling the outer mitochondrial membrane. This remodeling involves the assembly of M1- and K63-linked ubiquitin chains and the recruitment of ubiquitin-binding proteins and signaling components to the outer mitochondrial membrane, which obviously impedes Bax insertion into the outer membrane under proapoptotic conditions. Conceptually, this early TNF response ensures mitochondrial integrity and fitness to fulfill their role in signal amplification and transport of activated NF- $\kappa$ B to the nucleus. Along this line, maximal respiration and spare respiratory capacity were increased by TNF treatment.

Finally, our study unveiled a mitophagy-independent function of PINK1 in mitochondrial signaling. Previous studies already provided evidence for a role of PINK1 in NF- $\kappa$ B signaling. PINK1 was shown to increase Parkin-mediated K63-linked ubiquitination of NEMO *in vitro* and in cellular models and to increase TNF- and IL1-induced transcriptional activity of NF- $\kappa$ B (Sha *et al*, 2010; Akundi *et al*, 2011; Lee *et al*, 2012; Lee & Chung, 2012). Moreover, cytosolic PINK1 is stabilized by K63-linked ubiquitination in response to NF- $\kappa$ B pathway activation (Lim *et al*, 2015). In contrast to mitophagy-inducing conditions, PINK1 is stabilized in TNF signaling without dissipation of the mitochondrial membrane potential. Accordingly, proteolytically processed, mature PINK1 is stabilized in addition to full-length PINK1 destined for import through the TOM/TIM23 complexes. Albeit the accumulation of the mature PINK1 species after 15 min, TNF treatment is less striking than that of unprocessed PINK1 after 90 min CCCP treatment, several lines of evidence point toward a physiological role of PINK1 in NF- $\kappa$ B signaling. First, PINK1 phosphorylates M1-linked ubiquitin chains and thereby decreases the efficiency of OTULIN to hydrolyze linear ubiquitin chains. This explains why TNF-induced M1-ubiquitination is decreased in PINK1-deficient cells. Second, the fast anti-apoptotic TNF response depends on both HOIP and PINK1 expression. PINK1 is stabilized by complex formation with HOIP and HOIP-dependent linear ubiquitination and in turn augments M1-ubiquitination by antagonizing the disassembly of M1-linked ubiquitin chains. This scenario is reminiscent of the feed-forward activation loop in PINK1/Parkin-dependent mitophagy and completes the picture of a mitophagy-independent function of PINK1 and Parkin under physiological conditions that integrate their roles in innate immune signaling and stress protection.

## Materials and Methods

### Reagents and Tools table

Reagent or resource	Source	Identifier
<b>Antibodies</b>		
Rabbit monoclonal anti-cleaved caspase-3	Cell Signaling Technology	Cat#9664S
Mouse monoclonal anti-GAPDH	ThermoFisher Scientific	Cat#AM4300, RRID: AB_2536381
Rabbit polyclonal anti-HA	Sigma-Aldrich	Cat#H6908, RRID: AB_260070
Mouse monoclonal anti-HA	Covance Research Products Inc	Cat#NMS-101R, RIDD: N/A
Rabbit monoclonal anti-HA	Cell Signaling Technology	Cat#3724, RRID: AB_1549585
Rabbit polyclonal anti-HOIP (RNF31)	Bethyl	Cat#A303-560A, RRID: AB_10949139
Rabbit monoclonal anti-M1-ubiquitin (clone 1E3)	Millipore	Cat#MABS199, RRID: AB_2576212
Mouse monoclonal anti-NEMO	Santa Cruz Biotechnology	Cat#sc-8032, RRID: AB_627786
Rabbit polyclonal anti-OTULIN	Cell Signaling Technology	Cat#14127, RRID: AB_2576213
Rabbit polyclonal anti-IKK $\beta$	Cell Signaling Technology	Cat#2370, RRID: AB_2122154
Human polyclonal anti-M1-ubiquitin (clone 1F11/3F5/Y102L)	Genentech	1F11/3F5/Y102L
Mouse monoclonal anti-TNFR1	Santa Cruz	Cat#sc-8436, RRID: AB_628377
Mouse monoclonal anti-TIM23	BD Science	Cat#611222, RRID: AB_398755
Rabbit monoclonal anti-K63-ubiquitin	Millipore	Cat#05-1308, RRID: AB_1587580
Rabbit monoclonal anti-K48-ubiquitin	Cell Signaling Technology	Cat#8081, RRID: AB_10859893
Rabbit polyclonal anti-HOIL-1L (RBCK)	Invitrogen	Cat#PA5-11949, RRID: AB_2175271
Rabbit monoclonal anti-SHARPIN	Cell signaling Technology	Cat#12541, RRID: AB_2797949
Mouse monoclonal anti-Actin	Sigma-Aldrich	Cat#A5316, RRID: AB_476743
Goat polyclonal anti-HSP60	Santa Cruz	Cat#sc-1052, RRID: AB_631683
Rabbit polyclonal anti-VDAC	Cell Signaling Technology	Cat#4866, RRID: AB_2272627
Rabbit monoclonal anti-PINK1	Cell Signaling Technology	Cat#6946, RRID: AB_11179069
Mouse polyclonal anti-PINK1	Santa Cruz	Cat#sc-517353, RRID: N/A
Mouse monoclonal anti-V5	Invitrogen	Cat# R960-25, RRID: AB_2556564
Mouse monoclonal anti-ubiquitin	Santa Cruz	Cat# sc-8017, RRID: AB_628423
Rabbit anti-p-S65-ubiquitin	Fiesel et al (2015)	N/A
Rabbit polyclonal anti-Bax	Cell Signaling Technology	Cat#2772, RRID: AB_10695870
Rabbit monoclonal anti-cytochrome c	Cell Signaling Technology	Cat# 4280, RRID: AB_10695410
Rabbit monoclonal anti-NF- $\kappa$ B p65	Cell Signaling Technology	Cat# 8242, RRID: AB_10859369
Rabbit monoclonal anti-phospho-NF- $\kappa$ B p65 (S536)	Cell Signaling Technology	Cat# 3033, RRID: AB_331284
Rabbit polyclonal anti-IKBKG (NEMO)	Sigma-Aldrich	Cat# HPA000426, RRID: AB_1851572
Rabbit polyclonal anti-Optineurin (OPTN)	Sigma-Aldrich	Cat# HPA003279, RRID: AB_1079527
Rabbit polyclonal anti-Miro2	Proteintech	Cat# 11237-1-AP, RRID: AB_2179539



## Reagents and Tools table (continued)

Reagent or resource	Source	Identifier
Rabbit monoclonal anti-phospho TBK1/NAK (Ser172)	Cell Signaling Technology	Cat# 5483, RRID: AB_2798527
Mouse monoclonal anti-TOM20	Santa Cruz	Cat# sc-17764, RRID: AB_628381
Rabbit polyclonal anti-TOM70	Proteintech	Cat# 14528-1-AP, RRID: AB_2303727
Rabbit monoclonal anti-phospho-NF- $\kappa$ B p65 (Ser536)	ThermoFisher	Cat# MA5-15160 RRID: AB_10983078
Rabbit anti-p-S65-Parkin	Kane et al (2014)	
Strep-Tactin <sup>®</sup> HRP conjugate	IBA Lifesciences	Cat# 2-1502-001
<b>Biological samples</b>		
Human peripheral blood mononuclear cells	DRK-Blutspendedienst Baden-Württemberg—Hessen, Institut für Transfusionsmedizin und Immunhämatologie, Frankfurt, Germany	<a href="https://www.blutspende.de">https://www.blutspende.de</a>
Human serum	DRK-Blutspendedienst Baden-Württemberg—Hessen	<a href="https://www.blutspende.de">https://www.blutspende.de</a>
<b>Chemical, peptides, and recombinant proteins</b>		
Human TNF	Peptotech	Cat# 300-01A
Murine TNF	Peptotech	Cat# 315-01A
Staurosporine	Enzo life science	Cat# ALX 380-014M001
Carbonyl cyanide 3-chlorophenylhydrazone	Sigma-Aldrich	Cat# C2759
Antimycin A	Sigma-Aldrich	Cat# A8674
Oligomycin	Sigma-Aldrich	Cat# O4876
Tetra-ubiquitin (linear)	Enzo Life Sciences	Cat# BML-UW0785-0100
Recombinant human ubiquitin	Biotechne	Cat# U-100H-10M
<b>Cell lines</b>		
SH-SY5Y	Leibniz-Institut DSMZ-Deutsche Sammlung von Mikroorganismen und Zellkulturen GmbH <a href="https://www.dsmz.de/home.html">https://www.dsmz.de/home.html</a>	DSMZ no.: ACC 209
HEK293T	ATCC <a href="https://www.lgcstandards-atcc.org/">https://www.lgcstandards-atcc.org/</a>	ATCC <sup>®</sup> CRL-1573 <sup>™</sup>
HAP1 WT and HAP1 HOIP (RNF31) KO	Horizon	<a href="https://www.horizondiscovery.com">https://www.horizondiscovery.com</a>
HeLa	Leibniz-Institut DSMZ-Deutsche Sammlung von Mikroorganismen und Zellkulturen GmbH <a href="https://www.dsmz.de/home.html">https://www.dsmz.de/home.html</a>	DSMZ no.: ACC 57
<b>Oligonucleotides</b>		
OTULIN siRNA human: GGAAGAAUGAGGACCGGUUGAUAA GCGGAGAAUAGCCUCUAUGAAG UCUCCAAGUACAACACGGAAGAAU	Invitrogen	HSS131920 HSS131921 HSS131922
HOIP siRNA human: GGUACUGGCGUGGUGUCAAGUUAA, GAGAUGUCUGCGAUUAUUGGCUA, CACCACCCUCGAGACUGCCUCUUCU	Invitrogen	HSS123836 HSS123837 HSS182838
PINK1 siRNA human: GGACCGUUGUCCUGUUAUGAAGAA GGAGUACUGAUAGGGCAGUCCAU GAGUAGCCGCAAUGGCUUCAUCU	Invitrogen	HSS127945 HSS127946 HSS185707
RHOT1 siRNA human	GE Dharmacon	Cat# L-010365-01-0005, smartpool
RHOT2 siRNA human	GE Dharmacon	Cat# L-008340-01-0005, smartpool
PINK1-V5_K219A forward: 5'- CCCTTGCCATCGCGATGATGTGGA ACATCTCG-3'	This paper	N/A

Reagents and Tools table (continued)

Reagent or resource	Source	Identifier
PINK1-V5_K219A reverse: 5'- CGDGATGTTCCACATCATCGCGAT GGCCAAGGG-3'	This paper	N/A
PINK1-V5 D362A forward: 5'- GGCATCGCGCACAGAGCCCTGAAA TCCGAC-3'	This paper	N/A
PINK1-V5 D362A reverse: 5'- CTCGGATTCAGGGCTCTGTGCC GATGCC-3'	This paper	N/A
PINK1-V5 D384A forward: 5'- CTGGTGATCGCAGCTTTGGCTGCT GCTG-3'	This paper	N/A
PINK1-V5 D384A reverse: 5'- CAGGCAGCAGCCAAAAGCTGCGAT CACCG-3'	This paper	N/A
actin_forward: 5'- CCTGCCACCCAGCACAAT-3'	This paper	N/A
actin_reverse: 5'- GGGCCGGACTCGTCATAC-3'	This paper	N/A
PINK1 human forward: 5'- GTGGAACATCTCGCAGGT-3'	This paper	N/A
PINK1 human reverse: 5'- TTGCTTGGGACCTCTCTTGG-3'	This paper	N/A
Itprrip HindIII-FF: 5'-TTTAGTAAGCTTATGGCCATGGGGC TCTCCGC-3'	This paper	N/A
RV Itprrip XbaI Rev: 5'-AGTGCTTCTAGAGCTTTTGGGGTA GGCTGGTC-3	This paper	N/A
<b>Recombinant DNA</b>		
pET47b HOIP-RBR-LDD (C-terminal HOIP)	Stieglitz <i>et al</i> (2012)	N/A
pGEXP 6P1 tcPINK1 WT (a.a. 121–570)	Rasool <i>et al</i> (2018)	N/A
pET28a LIC UBE2L3	Stieglitz <i>et al</i> (2012)	N/A
pcDNA6A PINK1-V5	Exner <i>et al</i> (2007)	N/A
pcDNA6A PINK1-V5 kinase dead (K219A, D362A, D384A)	This paper	N/A
pcDNA6A PINK1 Δ77	This paper	N/A
pcDNA3.1 HA-HOIP	Muller-Rischart <i>et al</i> (2013)	N/A
pcDNA3.1 HA- (697–1,072) HOIP	Meschede <i>et al</i> (2020)	N/A
pcDNA3.1 HA- (1–697) HOIP	Meschede <i>et al</i> (2020)	N/A
pcDNA3.1 HA- (1–475) HOIP	Meschede <i>et al</i> (2020)	N/A
pcDNA3.1 HA- (1–408) HOIP	Meschede <i>et al</i> (2020)	N/A
pcDNA3.1 HA- (1–349) HOIP	Meschede <i>et al</i> (2020)	N/A
pcDNA3.1 HA- (1–298) HOIP	Meschede <i>et al</i> (2020)	N/A
pcDNA3.1 OTULIN WT	Stangl <i>et al</i> (2019)	N/A
pcDNA3.1 OTULIN W96A	Stangl <i>et al</i> (2019)	N/A
NF-κB luciferase	Krappmann <i>et al</i> (2001)	N/A
pcDNA3.1 HA-NEMO	This paper	N/A
pASK IBA 3+ Strep-OTULIN	This paper	N/A
pET28b His-mouseUBE1	Addgene	#32534

Reagents and Tools table (continued)

Reagent or resource	Source	Identifier
OMM-GFP <sub>1-10</sub> , GFP <sub>1-10</sub> , RFP-β11	Cieri et al (2018), Vallese et al (2020)	N/A
pcDNA3 ONM-β11	This paper	N/A
<b>Critical commercial assays</b>		
Duolink <sup>®</sup> <i>In Situ</i> PLA <sup>®</sup> Probe Anti-Rabbit PLUS	Sigma-Aldrich	#DUO92002
Duolink <sup>®</sup> <i>In Situ</i> PLA <sup>®</sup> Probe Anti-Mouse MINUS	Sigma-Aldrich	#DUO92004
Duolink <sup>®</sup> <i>In Situ</i> Detection Reagents Green	Sigma-Aldrich	#DUO92014
Duolink <sup>®</sup> <i>In Situ</i> Mounting Medium with DAPI	Sigma-Aldrich	#DUO82040
Seahorse XF Cell Mito Stress Kit	Agilent	#103015-100
Seahorse XF Real-Time ATP Rate Assay Kit	Agilent	#1035292-100

## Methods and Protocols

### DNA constructs

The wildtype PINK1-V5 construct was described previously (Exner et al, 2007). It was generated by cloning the human PINK1 cDNA into the pcDNA6 vector via NheI and XhoI. For cloning of the kinase dead PINK1-V5 mutant (K219A, D362A, D384A), the construct was modified by point mutations by using the indicated primers. For cloning of the PINK1-Δ77-V5 mutant, the PINK1 sequence 78–581 was cloned into pcDNA6 vector. Wildtype human HOIP, HOIL-1L, and SHARPIN were described previously (Muller-Rischart et al, 2013). HA-HOIP 1–697 was generated using the indicated primers and then incorporated into pcDNA 3.1-N-HA via EcoRI and XbaI. HA-HOIP ΔNZF1, HA-HOIP ΔNZF2, HA-HOIP ΔNZF1 + 2, HA-HOIP ΔUBA, and HA-HOIP ΔPUB were generated by overlap extension PCR (van Well et al, 2019; Meschede et al, 2020). The amplified fragments were generated using the primers indicated in the Materials section. The ONM-β11 construct has been amplified by PCR from the template pLV-EF1a-Itrprip-V5 (Addgene plasmid #120241; <http://n2t.net/addgene:120241>; RRID:Addgene\_120241) by using the following primers: Itrprip HindIII-FF and RV Itrprip XbaI Rev and cloned in pcDNA3 vector containing the short-β11 strand. The OMM-GFP<sub>1-10</sub> construct, the GFP<sub>1-10</sub> construct, and the RFP-β11 construct have been described previously (Cieri et al, 2018, Vallese et al, 2020).

### Cell culture

#### HEK293T, HeLa cells, mouse embryonic fibroblasts (MEFs)

Cells were cultured in Dulbecco's modified Eagle's medium (DMEM) supplemented with 10% (v/v) fetal bovine serum (FBS) and 100 IU/ml penicillin and 100 μg/ml streptomycin sulfate. PINK1-KO MEFs have been described previously (Muller-Rischart et al, 2013).

#### SH-SY5Y cells

Cells were cultured in Dulbecco's modified Eagle's medium F-12 (DMEM/F12) supplemented with 15% (v/v) fetal bovine serum (FBS), 100 IU/ml penicillin, 100 μg/ml streptomycin sulfate and 1× MEM nonessential amino acids solution (Gibco™).

#### HAP1 WT and HAP1 HOIP (RNF31) KO

Cells were cultured in Iscove's Modified Dulbecco's Medium (IMDM) supplemented with 10% (v/v) FBS, 100 IU/ml penicillin, 100 μg/ml streptomycin sulfate, and 8 mM L-glutamine.

#### Human primary macrophages

Human peripheral blood mononuclear cells (PBMC) were isolated from commercially available buffy coats from anonymous donors (DRK-Blutspendedienst Baden-Württemberg—Hessen, Institut für Transfusionsmedizin und Immunhämatologie, Frankfurt, Germany) using Pancoll (PAN Biotech, Aidenbach, Germany) density centrifugation. Monocytes were separated from PBMC by adherence to plastic after 1 h incubation in a serum-free RPMI1640 medium. To differentiate into macrophages, monocytes were cultured in RPMI1640 medium (ThermoFisher Scientific, Waltham, MA, USA) supplemented with 100 U/ml penicillin, 100 μg/ml streptomycin, and 3% human serum (DRK-Blutspendedienst Baden-Württemberg—Hessen) for 7 days followed by culture in RPMI 1640 medium containing 10% fetal calf serum.

Cultured cells were tested for mycoplasma contamination regularly every 3–4 months.

#### Transfection and siRNA knockdown

Unless described otherwise, transfections were performed using the following procedures: For SH-SY5Y and HeLa cells, Lipofectamine and Plus Reagent (Invitrogen) was used according to the manufacturer's instructions. For RNA interference, cells were transfected with stealth siRNA oligos (Invitrogen) using Lipofectamine RNAiMAX (Invitrogen) or Lipofectamine 2000 (Invitrogen) for co-transfection of siRNA oligos and DNA plasmids. HEK293T cells were transfected using PEI (polyethylenimine). DNA and PEI were mixed in a 1:2 ratio (μg:μl) in Opti-MEM and incubated for 15 min at room temperature. The DNA-PEI mixture was then added to the cells.

#### SPLIC<sup>NU-MT</sup> transfection

Transient transfection was performed using the calcium phosphate method. 30,000 HeLa cells/well were seeded on a 24-well plate on

coverslips in the evening. The morning after, a transfection mixture was prepared as follows (quantities reported per well): 50  $\mu$ l HEPES buffered saline 2x (Merck), 5  $\mu$ l 2.5 M CaCl<sub>2</sub>, 1 + 1  $\mu$ g SPLICS<sup>NU-MT</sup> plasmids, and up to 100  $\mu$ l sterile H<sub>2</sub>O. The mixture was added to the wells, each containing 500  $\mu$ l of growth medium. After 8 h, the mixture-containing medium was removed and replaced with a fresh medium. 24 h after a medium change, the cells were treated as described below and fixed.

#### SPLICS<sup>NU-MT</sup> and siRNA co-transfection

Co-transfection of SPLICS<sup>NU-MT</sup> plasmids and siRNAs for HOIP silencing was performed using Lipofectamine 3000 (Thermo Fisher). 400,000 HeLa cells/well were seeded on a 6-well plate in the evening. The morning after, the medium was replaced with 750  $\mu$ l/well Opti-MEM (Thermo Fisher), and a transfection mixture with the following composition per well was prepared and added to the wells: 250  $\mu$ l Opti-MEM, 0.5 + 0.5  $\mu$ g SPLICS<sup>NU-MT</sup> plasmids, 60  $\mu$ M each (180  $\mu$ M in total) stealth siRNA oligos (Invitrogen), and 5  $\mu$ l Lipofectamine 3,000. 32 h after the addition of the transfection mixture, the cells were detached using trypsin and re-seeded on a 24-well plate on coverslips (30,000 cells/well). 16 h after the re-seeding, the cells were treated as described below and fixed.

#### Immunoblotting

Proteins were size-fractionated by SDS-PAGE and transferred to nitrocellulose or polyvinylidene difluoride membranes by electroblotting. The nitrocellulose membranes were blocked with 5% nonfat dry milk or 5% BSA in TBST (TBS containing 0.1% Tween 20) for 60 min at room temperature and subsequently incubated with the primary antibody diluted in blocking buffer for 16 h at 4°C. After extensive washing with TBST, the membranes were incubated with horseradish peroxidase-conjugated secondary antibody for 60 min at room temperature. Following washing with TBST, the antigen was detected with the enhanced chemiluminescence (ECL) detection system (Promega) as specified by the manufacturer. In addition, immunoblots with fluorescently labeled secondary antibodies were imaged by an Azure Sapphire Biomolecular Imager (Azure Biosystems, USA). For quantification of Western blots, Image Studio lite (version 3.1) and Fiji were used for X-ray films and AzureSpot (version 2.0) was used for the Sapphire Biomolecular Imager (Azure Biosystems, USA).

#### Mitochondrial bioenergetics

Metabolism of living cells was measured in real-time using Seahorse XF 96 Analyzer. The Seahorse Cell Mito Stress Test was employed to measure basal mitochondrial respiration, maximal mitochondrial respiration, and spare respiratory capacity. The Seahorse Real-Time ATP Rate Assay was used to measure mitochondrial and glycolytic ATP production rates in living cells. A Seahorse 96-well cell culture microplate was coated with poly-L-lysine for 10 min before seeding HeLa cells as a density of  $1 \times 10^4$ . The outer rim of the plates was used for background correction, containing only medium without cells. HeLa cells were incubated for 48 h at 37°C, 5% CO<sub>2</sub> in cell culture media before the assay was started. Sensor cartridge was hydrated 1 day prior to sample analysis by sterile H<sub>2</sub>O at 37°C in a CO<sub>2</sub>-free incubator. One to two hours before starting the analysis, water was replaced by 200  $\mu$ l of prewarmed Seahorse XF Calibrant per well. All assay compounds (oligomycin, FCCP, rotenone, and

antimycin A) were solubilized in DMSO to a stock concentration of 5 mM and stored at -20°C. On the day of the assay, compounds were prepared for loading in XF sensor cartridge. Concentrations were chosen according to the Seahorse assay performed. Stock solution of compounds was mixed with an assay medium to generate 10 $\times$  port concentrations. Compounds were loaded into ports in XF sensor cartridge. XF sensor cartridge plate was placed into the Seahorse XF 96 analyzer and calibration was performed. Afterward, the calibration plate was replaced by the XF cell culture microplate and measurement was started. Prewarmed Seahorse DMEM assay media (pH 7.4) was supplied with 10 mM glucose, 2 mM L-glutamine, and 1 mM pyruvate. Cells were washed once with Seahorse assay media before 180  $\mu$ l of Seahorse assay media was added to each well. Cells were incubated at 37°C in a non-CO<sub>2</sub> incubator for 45–60 min prior to the assay. For the XF Real-Time ATP Rate Assay performed with HeLa cells, Seahorse DMEM assay media was exchanged again before starting the assay. The analysis of Seahorse Assays was performed by Wave Software. Data values were exported to Excel and further analyzed as described in User Manuals. For the Seahorse Real-Time ATP Rate Assay, the Seahorse Report Generator in Excel was used. Statistical Analysis was performed using GraphPad PRISM (GraphPad Software, San Diego California, USA).

#### Expression and purification of recombinant proteins

Bacterial expression and purification of GST-tagged proteins (C-terminal HOIP, M1-linked tetra-ubiquitin, tcPINK1), Strep-tagged proteins (OTULIN and UBAN domain), and His-tagged proteins (mouse UBE1 and UBE2L3) were performed by standardized methods (Stieglitz *et al*, 2012; Rasool *et al*, 2018). The proteins were expressed in *E. coli* BL21 (DE3)-pLys to an OD 600 of 0.6–0.8 before induction with 0.1 mM isopropyl- $\beta$ -D-thiogalactopyranoside and a change in temperature to 18°C overnight. In the case of C-terminal HOIP, the medium was supplemented with 150  $\mu$ M ZnCl<sub>2</sub>. Cells were harvested and resuspended in 20 mM Tris-Cl pH 7.5, 150 mM NaCl, 10% glycerol, and 1 mM DTT and lysed by a French press. After centrifugation for 40 min at 38,000 g, tagged proteins were affinity-purified with a HisTrap HP nickel column (GE Healthcare) or glutathione Sepharose 4B resin (GE Healthcare) or StrepTrap XT (Cytiva). For further purification, exclusion chromatography (HiLoad 16/600 Superdex 75 pg, Cytiva) or anionic exchange (HiTrap Capto Q, Cytiva) was performed. In all purification steps, the eluates were collected, and SDS-PAGE was performed to determine the protein purity. The protein concentration was determined using the absorbance at 280 nm and the extinction coefficient of each construct by Nanodrop (Thermo Fisher). Recombinant ubiquitin was purchased from Sigma-Aldrich (79586-22-4).

#### Quantitative RT-PCR

Total cellular RNA was isolated with the RNeasy Mini Kit (Qiagen) according to the manufacturer's instructions. 1,000 ng RNA was reverse-transcribed into cDNA using the iScript<sup>TM</sup> cDNA Synthesis Kit (Bio-RAD, CA, USA). cDNA was diluted 1:5 in PCR-grade dH<sub>2</sub>O and 1.5  $\mu$ l of the cDNA-mix was used per 20  $\mu$ l real-time PCR reaction with 0.25  $\mu$ M of each primer and 2 $\times$  FastStart Essential DNA Green Master Mix (Roche). For each target and reference gene, samples were run in triplicates on a Light Cycler 96 (Roche). On each plate, relevant negative controls were run. Melt curves were studied for all assays, with the T<sub>m</sub> checked to be within known

specifications for each assay. Standard curves were run for each primer pair. Relative quantification of PINK1 mRNA was performed using the  $2^{-\Delta\Delta C_T}$  method.

### Immunocytochemistry

SY-SY5Y, HAP1, MEFs, and neuronal cells were cultivated on glass coverslips (Laboratory Glassware Marienfeld). 24–72 h after transfection, cells were washed with PBS pH 7.4, fixed for 15 min with 4% paraformaldehyde in PBS pH 7.4, and permeabilized with 0.2% (v/v) Triton X-100 in PBS for 10 min or with 0.5% saponin, 1% BSA in PBS for 45 min at room temperature. After blocking with 1% BSA or 5% goat/donkey serum, the cells were stained with primary antibodies at a dilution of 1:100 to 1:1,000 in PBS or 0.5% saponin, 1% BSA in PBS at 4°C overnight, washed with PBS and incubated with fluorescent dye-conjugated secondary antibodies AlexaFluor488, 555 or 647 (Thermo Scientific), at a dilution of 1:1,000 for 1 h at room temperature. Cells were washed with PBS pH 7.4 three times and subsequently incubated with DAPI (1 µg/ml) in H<sub>2</sub>O. Following a final wash in H<sub>2</sub>O, cells were mounted in Fluoromount G (Thermo Fisher Scientific).

### Proximity ligation assay

*In situ* proximity ligation assays were performed using the Duolink<sup>®</sup> PLA (Sigma-Aldrich). The protocol was adapted from the manufacturer's instruction. Before fixation, cells were stained with MitoTracker<sup>™</sup> Red CMXRos Dye (1:10,000) for 30 min at 37°C. After fixation and permeabilization according to the immunocytochemistry protocol, cells were incubated with blocking solution provided in the Duolink<sup>®</sup> kit for 1 h at 37°C followed by incubation with primary antibodies diluted in the Duolink<sup>®</sup> antibody diluent overnight at 4°C. After washing the cells three times for 5 min in wash buffer A, the cells were incubated with the PLA probes anti-mouse Minus and anti-rabbit Plus, diluted 1:5 in the Duolink<sup>®</sup> antibody diluent in a preheated humidity chamber for 1 h at 37°C. After washing the cells three times for 5 min in wash buffer A, ligation and amplification were performed with the Duolink<sup>®</sup> *in situ* detection reagents green following the manufacturer's protocol. After the final washing steps in 0.01× wash buffer B, the coverslips were mounted with the Duolink<sup>®</sup> mounting media. For negative controls, only one primary antibody was used for incubation. For positive controls, mouse anti-TOM20 and rabbit anti-TOM70 antibodies were incubated in parallel.

### Mitochondrial and nuclear staining in SPLICS<sup>NU-MT</sup> transfected cells

Cells were fixed with 3.75% paraformaldehyde in PBS for 20 min, permeabilized with 0.3% Triton X-100 for 10 min, blocked with 1% bovine gelatin in PBS for 10 min three times, and then washed with PBS for 5 min three times. Mitochondria were stained using a 1:100-diluted rabbit anti-TOM20 primary antibody (Santa Cruz). Cells were incubated with the antibody in a wet chamber for 2 h at room temperature, blocked three times with gelatin in PBS for 10 min, and washed three times with PBS for 5 min. Cells were then incubated with a 1:100-diluted AlexaFluor 594-conjugated anti-rabbit secondary antibody (ThermoFisher) in a wet chamber for 45 min at room temperature, rinsed with gelatin in PBS for three times, then nuclei were stained by incubating the cells with 1 µg/ml Hoechst

33342 in PBS for 10 min. Finally, the cells were washed three times with PBS for 5 min and mounted on glass slides before being analyzed by a Zeiss sp5 confocal microscope.

### Assessment of the mitochondrial membrane potential

For  $\Delta\Psi_m$  determination, HeLa cells were stained with 7 nM tetramethylrhodamine ethyl ester perchlorate (TMRE). For ratiometric imaging, dual staining was performed with MitoTracker Green FM (MTG), used at a concentration of 100 nM. MTG is a  $\Delta\Psi_m$  independent dye. TMRE is rapidly equilibrated and nontoxic for respiration in those low concentrations. Cells grown on glass coverslips were stained in fresh medium for 30 min at 37°C with 100 nM MitoTracker<sup>®</sup> Green FM, washed once with PBS and once with medium, and then imaged in fresh media containing 7 nM TMRE and 10 µM verapamil (after another 30 min of incubation). MTG emission was recorded between 500 and 510 nm. TMRE was added 30 min before the measurements and kept in a medium throughout the experiments. During imaging, no MTG was present in the medium. TMRE was obtained from Biomol GmbH and MTG from ThermoFisher Scientific. Determination of  $\Delta\Psi$  was performed by simultaneous TMRE and MTG measurements (Z-stacks, 0.25 nm steps, seven slices) to enable normalization according to Wikstrom *et al* (2007) with a cLSM (Leica SP8) equipped with a tunable white light laser (470–670 nm), a 63× water objective (N.A. 1.2) and two highly sensitive hybrid GAsP (HyD) detectors. Two technical replicates were conducted. For evaluation, an Otso mask was used to obtain the mitochondria skeleton only. Mean gray values were determined for each cell, and the fluorescence emission ratio (TMRE/MTG) was calculated. Box-and-whisker plot from mean gray value data points (each data point represents the mean of one cell = one mitochondrial network). Error bars denote 5<sup>th</sup> to 95<sup>th</sup> percentile values, boxes represent 25<sup>th</sup> to 75<sup>th</sup> percentiles. Vertical lines in boxes represent the median values, whereas square symbols in boxes denote the respective mean values. Minimum and maximum values are denoted by x. Significance levels were determined by a one-way ANOVA: \* $P \leq 0.05$ ; \*\* $P \leq 0.01$ ; \*\*\* $P \leq 0.001$ .

### Live-cell imaging of mitochondrial movement

SH-SY5Y were plated on a 35 mm Ibidi Glass Bottom dish at a concentration of  $2 \times 10^5$  cells per dish. 48 h after seeding, cells were incubated with 1× NucSpot<sup>®</sup> Live 488 (Biotium Inc., USA) and 1× MitoView<sup>®</sup> Fix 640 (Biotium Inc., USA) for 30 min at 37°C prior to imaging. TNF was added immediately before starting the image acquisition. Imaging was carried out using an Elyra 7 Lattice-SIM Super-Resolution microscope (Zeiss, Oberkochen, Germany) every 2 min for 30 min with a 63× oil objective (Plan-Apochromat 63×/NA1.4). Image analysis was performed with Imaris 9.9.1 (Bitplane AG, Switzerland) using the Spot (mitochondria) and surface (nucleus) functions. Mitochondrial shortest distance to the nucleus is color-coded.

Macrophages were plated on at 50,000 cells/well in µ-Slide 8-well chambers (80826, Ibidi, Martinsried, Germany) and incubated with 0.5 µM MitoTracker Green (Thermo Fisher Scientific) for 15 min at 37°C prior to imaging. The nuclei were stained using 2 µM Hoechst (Thermo Fisher Scientific). TNF was added immediately before starting video recording. Imaging was carried out using a confocal microscope (LSM800, Carl Zeiss, Oberkochen, Germany) and LD Plan-Apochromat 40× objective.

### Electron microscopy

Cell grown on ACLAR<sup>®</sup>-Fluoropolymer fil (Plano) were fixed by immersion using 2% glutaraldehyde in 0.1 M cacodylate buffer at pH 7.4 overnight at 4°C. After postfixation in 1% osmium tetroxide and pre-embedding staining with 1% uranyl acetate, tissue samples were dehydrated and embedded in Agar 100. Thin sections (80 nm) were counterstained using 1% uranylacetat (aq) and examined using a Talos L120C (Thermo Fisher Scientific).

### Flow cytometry

Flow cytometry was performed on a BD FACSymphony A5 cell analyzer. HeLa FlpIn TRex cells stably expressing mt-mKEIMA and doxycycline-inducible Parkin were seeded in 6-well plates 48 h prior to treatment. Parkin expression was induced for 24 h by 0.25 µg/ml doxycycline. Cells were treated with TNF or antimycin A/oligomycin (10 µM) for the indicated time (25 ng/ml for 30 min or 10 ng/ml for 16 h) and harvested by Trypsin digestion. 10,000 events were preselected for viable, fluorescent, single cells. Dual-fluorescence for 405 nm (mt-mKEIMA pH 7) and 561 nm (mt-mKEIMA pH 4) excitation and 610/20 nm emission was recorded. The ratio between 561 and 405 nm mt-mKEIMA fluorescence is a measure of mitophagic flux.

### Mitochondria fractionation

To extract crude mitochondria, cells were washed with ice-cold PBS buffer 2 times and scraped from the dishes. Cells were then collected and centrifuged at 1,000 g for 1 min at 4°C. Cell pellets were resuspended in RSB buffer (10 mM Tris-HCl, 10 mM NaCl, 1.5 mM CaCl<sub>2</sub>, pH 7.4) for 2–3 min on ice to swell, and then centrifuged at 2,400 g for 5 min at 4°C. The pellets were resuspended in 1:1 mixed RSB/MS buffer (420 mM mannitol, 140 mM sucrose, 10 mM Tris-HCl, 5 mM EDTA, pH 7.4 protease inhibitors, phosphatase inhibitors, N-ethylmaleimide) and lysed with a 23 G needle (10 times) followed by a 26 G needle (5 times). For human macrophages, the cell suspension was lysed with a 30 G needle (5 times) in addition. The lysed cell suspension was diluted 1:1 ratio with MS buffer. The lysates were centrifuged at 1,500 g for 15 min at 4°C. The supernatant was collected and centrifuged at 14,000 g for 15 min at 4°C to sediment crude mitochondria. The supernatant was centrifuged at 20,000 g for 1 h at 4°C to collect purified cytosol. For further purification, the crude mitochondria were resuspended in 36% Opti-prep solution and transferred to a tube, overlaid with 4 ml 30% Opti-prep solution and 4 ml 10% Opti-prep solution. 1 ml diluent (250 mM sucrose, 6 mM EDTA, 120 mM HEPES, pH 7.4) was added on top of the gradient. The Opti-prep gradients were centrifuged at 213,000 g for 4 h at 4°C. After centrifugation, the white fluffy layer between 30 and 10% was collected and diluted with M1 buffer (600 mM sucrose, 50 mM Tris-HCl, 10 mM EDTA, pH 8.0), centrifuge at 14,000 g for 10 min at 4°C to sediment purified mitochondria.

### Linear ubiquitination assay

Cells were lysed in denaturing lysis buffer (1% SDS in PBS) and heated (95°C for 10 min). Protein extracts were diluted 1:10 with nondenaturing lysis buffer (1% Triton X-100 in PBS) and cleared by centrifugation. To pull down proteins modified by linear ubiquitin chains, 20 µg of the recombinant UBAN domain of NEMO was added, which carries an N-terminal Strep-Tag II. After incubation

for 1 h at 4°C, Strep-Tactin beads were added and incubated overnight at 4°C. Beads were collected by centrifugation and washed. Laemmli sample buffer was added, and the samples were boiled for 10 min. Proteins binding to the UBAN domain were separated with SDS-PAGE and analyzed by immunoblotting using antibodies against M1- ubiquitin or pan-ubiquitin (in case OTULIN was used as a control for M1-ubiquitin specificity).

### Co-immunoprecipitation

Cells were harvested in cold PBS and subsequently lysed in 1% (v/v) Triton X-100 in PBS supplemented with Protease Inhibitor Cocktail (Roche), N-ethylmaleimide and sodium orthovanadate. The lysates were cleared by centrifugation at 20,000 g and incubated overnight with anti-HA agarose beads at 4°C with gentle rotation. Beads were washed three times with lysis buffer. Immunopurified proteins were eluted by adding Laemmli sample buffer (LSB) and boiling for 10 min.

For endogenous PINK1 immunoprecipitation, crude mitochondria were extracted from cells and lysed in 1% Triton X-100 lysis buffer on ice for 5 min, then centrifuged at 20,000 g for 20 min at 4°C. The lysates were incubated with rabbit anti-PINK1 antibody or IgG epitope control overnight at 4°C. The samples were then incubated with prewashed protein A beads for 3 h. The protein A beads were washed with 1% Triton X-100 lysis buffer 3 times before adding to the samples. The beads were washed three times with 1% Triton X-100 lysis buffer, finally eluted with 2× LSB, and analyzed by Western blotting.

### Size-exclusion chromatography

HEK293T cells expressing PINK1-V5 were lysed in Tris buffer (50 mM Tris-pH 7.5, 1 mM MgCl<sub>2</sub>, 1 mM DTT, and complete protease inhibitor) by repeated passing through a syringe needle. After 15 min incubation on ice, lysates were cleared by centrifugation (20,000 g, 20 min, 4°C). Protein concentration of the samples was measured by the Bradford protein assay and equal amounts of proteins were loaded on the column. Proteins were separated on a Superdex 200 10/300 GL column using an ÄKTA chromatography system (GE Healthcare Life Sciences). 0.5 or 1 ml fractions were collected and analyzed by Western blotting using antibodies against HOIP and the V5 tag.

### In vitro ubiquitination assay

PINK1 was immunoprecipitated from cell lysates by anti-V5 beads. The beads were washed three times with 1% Triton X-100 lysis buffer and twice with ubiquitination reaction buffer (50 mM Tris-HCl, 5 mM MgCl<sub>2</sub>, 0.5 mM TCEP), and then incubated with recombinant ubiquitin (30 µM), mouse Ube1 (0.1 µM), UBE2L3 (1 µM), C-terminal HOIP (4 µM) and ATP (2 mM) in the *in vitro* ubiquitination reaction buffer for 90 min at 30°C. Reactions were terminated by adding 5× LSB into the reaction mix at 97°C for 3 min. Samples were analyzed by Western blotting.

### In vitro deubiquitination assay

Recombinant M1-linked tetra-ubiquitin (2.5 µg) was incubated with or without 16 µg tcPINK1 or 16 µg BSA as a control for 48 h at 30°C in kinase buffer (500 mM Tris, 100 mM MgCl<sub>2</sub>, 10 nM ATP, 10 mM DTT). For the DUB assay, 0.26 µg recombinant OTULIN was added and incubated at 37°C for the indicated time. The DUB reaction was

terminated by 5× LSB and heating (80°C). The samples were analyzed by immunoblotting and Phos-tag™ PAGE.

### Cellular deubiquitination assay

PINK1 was immunoprecipitated from cellular lysates as described above and the beads were resuspended in low salt buffer containing recombinant OTULIN (2 mM) and incubated at 25°C for 1 h. The reaction was terminated by adding 5× LSB and heating (95°C). The samples were analyzed by Western blotting.

### Apoptosis assays

Activated caspase-3 was quantified as described previously (Meschede *et al.*, 2020). In brief, cells plated on glass coverslips were stained with antibodies against activated caspase-3 by indirect immunofluorescence, and signals were visualized by fluorescence microscopy using a Nikon Eclipse E400 microscope.

For the assessment of Bax recruitment, mitochondrial fractions were analyzed by immunoblotting using Bax-specific antibodies. For analyzing cytochrome *c* release, subcellular fractionation was performed by differential centrifugation. The cytosolic and mitochondrial fractions were analyzed by immunoblotting using antibodies against cytochrome *c*.

### Image acquisition

Fluorescence microscopy was performed using a Zeiss ELYRA PS.1 equipped with an LSM880 (Carl Zeiss, Jena) and a 20×, 63× oil, or 100× oil immersion objective or a C2+ system (Nikon). Super-resolution images were generated by structured illumination microscopy (SIM) using 405, 488, and 561 nm widefield laser illumination. SIM confocal images were processed using the ZEN2.3 software (Carl Zeiss, Jena). For the p65 translocation assay, laser scanning microscopy was performed using the 405, 488, and 561 laser illumination set in individual channels to avoid cross-talk. For live-cell experiments, imaging was carried out using an ELYRA 7 Lattice-SIM Super-Resolution microscope (Zeiss, Oberkochen, Germany) equipped with a 63× oil objective (Plan-Apochromat 63×/NA1.4).

### Image analysis

#### Mitochondrial movement

For the analysis of mitochondrial movement, cells were incubated with MitotrackerGreen™ (50 nM) and Hoechst (5 µg/ml) and imaged every 30 s after treatment with TNF (25 ng/ml). Mitochondria and the nucleus were segmented using Imaris 9.8 Surface and Spot modules and mitochondrial spots were classified with respect to the nuclear distance.

#### Cytosolic/nuclear ratio of the p65 signal

HeLa cells were plated on glass coverslips and transfected with control or Miro1- and Miro2-specific siRNAs. 48 h after transfection, the cells were treated with TNF (25 ng/ml) for 15 min and then fixed with 4% PFA in PBS for 10 min at room temperature. Cells were permeabilized with 0.2% Triton X-100 for 30 min and blocked with 5% donkey or goat serum in 0.2% Triton X-100 in PBS for 1 h at room temperature. Subsequently, the cells were incubated with an anti-p65 and anti-tubulin antibody diluted in a blocking buffer overnight at 4°C. After washing, the cells were incubated with AlexaFluor488 and AlexaFluor555 secondary antibodies for 1 h at room

temperature. Finally, the cells were washed extensively with PBS and then mounted onto glass slides and analyzed by laser scanning microscopy (LSM). For the analysis of the signal intensity ratio between the cytosol and the nucleus, LSM datasets including stainings for the whole cell (tubulin), p65, and the nucleus (DAPI) were exported using Zeiss Zen Blue (2.1). Based on the individual channels, datasets were segmented in a cytoplasmic and nuclear compartment and the fluorescence p65 signal intensity ratio for every cell was measured using CellProfiler 4.2.1.

Alternatively, the translocation of p65 from the cytosol to the nucleus was determined by indirect immunofluorescence based on single-cell analysis. SH-SY5Y cells or MEFs were plated on glass coverslips and transfected with control or PINK1-specific siRNA. For rescue experiment, cells were co-transfected with WT PINK1, PINK1Δ77, or kinase-dead PINK1-K/D mutant. Two days after transfection, the cells were treated with TNF (25 ng/ml, 25 min) and then fixed with 4% PFA in PBS for 10 min at room temperature. Cells were permeabilized with 0.2% Triton X-100 for 10 min and blocked with 5% donkey or goat serum in 0.2% Triton X-100 in PBS for 1 h at room temperature. Subsequently, the cells were incubated with an anti-p65 antibody diluted in a blocking buffer overnight at 4°C. After extensive washing, cells were incubated with an ALEXA488-conjugated secondary antibody for 1 h at room temperature. Finally, the cells were washed extensively with PBS and then mounted onto glass slides and analyzed by fluorescence microscopy using a Nikon Eclipse E400 microscope. Nuclei were counterstained with DAPI (Sigma) and transfected cells were visualized by EGFP or mCherry plasmid co-transfection.

### Mitochondrial ultrastructure

High-resolution images of mitochondria were imported into Imaris 9.8, and the scale was adjusted using the correct pixel sizes. For the analysis of average cristae number/mitochondrial area, Imaris 9.8 surface function was used, and for the average cristae length, data were collected using a direct measure function.

### Proximity ligation assay (PLA) positive foci quantification

To analyze the PLA-positive foci, the images were captured through laser scanning microscopy. Captured images were segmented with cytoplasmic and nucleus compartment, and the PLA foci were identified and counted through Cell Profiler 3.1.9.

### Mass spectrometry-based analysis for the identification of OTULIN interaction partners

In-gel digestion was performed as previously described (Sima *et al.*, 2021). 200 ng tryptic peptides were subsequently measured by nano-LC-ESI-MS/MS. An UltiMate 3000 RSLC nano-LC system (Thermo Scientific, Bremen, Germany) was utilized for nano-HPLC analysis using the following solvent system: (A) 0.1% FA; (B) 84% ACN, 0.1% FA. Samples were loaded on a trap column (Thermo, 100 µm × 2 cm, particle size 5 µm, pore size 100 Å, C18) with a flow rate of 30 µl/min with 0.1% TFA. After sample concentration and washing, the trap column was serially connected with an analytical C18 column (Thermo, 75 µm × 50 cm, particle size 2 µm, pore size 100 Å), and the peptides were separated with a flow rate of 400 nl/min using a solvent gradient of 4% to 40% B for 98 min at 60°C. After each sample measurement, 1 h of column washing was performed for equilibration. The HPLC system was online connected to the nano-

electrospray ionization source of an LTQ Orbitrap Elite mass spectrometer (Thermo Scientific, Bremen, Germany). The mass spectrometer was operated in a data-dependent mode with the spray voltage set to 1,600 V in positive mode and a capillary temperature of 275°C. Full scan MS spectra (mass range 300–2,000  $m/z$ ) were acquired in the Orbitrap analyzer at a mass resolution of 60,000. The 20 most intensive ions per spectra were subsequently fragmented using collision-induced dissociation (35% normalized collision energy) and scanned in the linear ion trap. The  $m/z$  values triggering MS/MS were set on a dynamic exclusion list for 30 s.

Proteins were identified and quantified using MaxQuant (v. 1.6.17.0, <https://maxquant.org/>) using Andromeda as a search engine. Spectra were matched against UniProt/Swiss-Prot using human taxonomy (released 2021\_02). Methionine oxidation was set as variable modifications; cysteine carbamidomethylation was a fixed one. The minimum number of peptides and razor peptides for protein identification was 1; the minimum number of unique peptides was 0. Protein identification was performed at a protein false discovery rate of 0.01. The “match between runs” option was on. Intensity-based absolute quantification (iBAQ) was used to estimate protein abundances (Tyanova *et al*, 2016). The Gene Ontology Cellular Compartment (GOCC) annotation was performed using DAVID Bioinformatics Resources 6.8 (Huang *da et al*, 2009a,b). Factory settings were maintained. Resulting tables were exported into excel, and the number of proteins from the identified cellular compartments were visualized in the pie chart.

### Quantification and statistical analysis

For the quantification of mitochondria-nucleus contact sites, Image analysis and contacts quantification was carried on using the ImageJ distribution Fiji (<https://imagej.net/software/fiji/>), ImageJ plugin VolumeJ, and custom macros were written for interorganelle contacts analysis. The analysis was done as previously described (Cali & Brini, 2021). An ROI was traced around the nucleus of probe-positive cells to quantify only contacts that involve the nuclear envelope.

Data represent the mean  $\pm$  SD or SEM,  $n$  numbers are indicated in the figure legends. For the quantification analysis in which manual counting was used, not all experiments were performed in a blinded manner. All statistical analyses were performed by using GraphPad PRISM (Version 5; San Diego, CA, USA) with the exception of mitochondria-nucleus contact sites, which were assessed by GraphPad Prism 8. To check the normal distribution of data, the Kolmogorov–Smirnov test was applied. Based on the outcome of the test, appropriate parametric and nonparametric tests were chosen. For the comparison of two independent parametric datasets, the student's  $t$ -test was used. For the comparison of more than 2 parametric datasets, one-way ANOVA was applied. To correct for  $\alpha$ -error inflation resulting from multiple comparisons, ANOVA was followed by the Tukey's *post hoc* multiple comparison tests. For the direct comparison of two nonparametric datasets, the Wilcoxon Mann–Whitney ( $U$ -test), and for the comparison of more than 2 nonparametric datasets, the Kruskal–Wallis test was used. Significance levels for all tests: \* $P \leq 0.05$ ; \*\* $P \leq 0.01$ ; \*\*\* $P \leq 0.001$ .

## Data availability

This study includes no data deposited in external repositories.

Expanded View for this article is available [online](#).

### Acknowledgement

We thank Jean-François Trempe for providing the tcPINK1 plasmid, Katrin Rittinger and Ben Stieglitz for the HOIP-RBR-LDD and UBE2L3 plasmids, Richard Youle for the p-S65-Parkin antibody, Daniel Krappmann for the OTULIN plasmids, Sadasivam Jegannathan for protein expression and purification, and Genentech for the 1F11/3F5/Y102L antibody. We also thank Günther Meschke for stimulating discussions. KFW is supported by the German Research Foundation (WI/2111-4, WI/2111-6, WI/2111/8, FOR 2848, and Germany's Excellence Strategy—EXC 2033-390677874—RESOLV) and the Michael J. Fox Foundation for Parkinson's Research (Grant IDs 16293 and 021968). SR-SIM microscopy was funded by the German Research Foundation and the State Government of North Rhine-Westphalia (INST 213/840-1 FUGG). TC is supported by grants from the Ministry of University and Research (Bando SIR 2014 no. RBSI14C65Z and PRIN2017) and from the Università degli Studi di Padova (Progetto Giovani 2012 no. GRIC128SP0 to T.C., Progetto di Ateneo 2016 no. CALI\_- SID16\_01, STARS Consolidator Grant 2019). M.B is supported by Local Funds from the University of Padova. CM is supported by the German Research Foundation (Project-ID 390339347, Emmy Noether Programme and Project-ID 259130777, CRC1177). WS is supported by the National Institutes of Health (NS085070, NS110085, and NS110435), the Department of Defense Congressionally Directed Medical Research Programs (W81XWH-17-1-0248), the Michael J. Fox Foundation for Parkinson's Research, Mayo Clinic Foundation and the Center for Biomedical Discovery (CBD).

### Author contributions

**Konstanze F Winklhofer:** Conceptualization; supervision; funding acquisition; visualization; writing – original draft; project administration; writing – review and editing. **Zhixiao Wu:** Formal analysis; validation; investigation; visualization; methodology; writing – original draft. **Lena A Berlemann:** Formal analysis; validation; investigation; methodology. **Verian Bader:** Formal analysis; supervision; validation; investigation; visualization; methodology; writing – original draft. **Dominik A Sehr:** Formal analysis; validation; investigation; visualization; methodology. **Eva Dawin:** Formal analysis; validation; investigation; visualization; methodology. **Alberto Covallero:** Formal analysis; validation; investigation; visualization. **Jens Meschede:** Formal analysis; validation; investigation; visualization. **Lena Angersbach:** Formal analysis; validation; investigation; visualization. **Cathrin Showkat:** Formal analysis; validation; investigation; visualization. **Jonas B Michaelis:** Formal analysis; validation; investigation; visualization. **Christian Münch:** Resources; supervision; validation. **Bettina Rieger:** Formal analysis; validation; investigation; visualization. **Dmitry Namgaladze:** Resources; formal analysis; investigation. **Maria Georgina Herrera:** Resources; formal analysis; investigation. **Fabienne C Fiesel:** Resources. **Wolfdieter Springer:** Resources. **Marta Mendes:** Formal analysis; investigation. **Jennifer Stepien:** Formal analysis. **Katalin Barkovits:** Formal analysis; validation; visualization; methodology; writing – original draft. **Katrin Marcus:** Formal analysis; supervision; methodology. **Albert Sickmann:** Supervision; methodology. **Gunnar Dittmar:** Formal analysis; supervision; visualization; methodology. **Karin B Busch:** Formal analysis; supervision; investigation; visualization; methodology. **Dietmar Riedel:** Supervision; investigation; visualization; methodology. **Marisa Brini:** Resources; supervision; methodology; writing – original draft. **Jörg Tatzelt:** Conceptualization; supervision; writing – original draft; project administration. **Tito Cali:** Resources; formal analysis; supervision; visualization; methodology; writing – original draft.



## Disclosure and competing interests statement

The authors declare that they have no conflict of interest.

## References

- Ablasser A, Hur S (2020) Regulation of cGAS- and RLR-mediated immunity to nucleic acids. *Nat Immunol* 21: 17–29
- Akundi RS, Huang Z, Eason J, Pandya JD, Zhi L, Cass WA, Sullivan PG, Bueler H (2011) Increased mitochondrial calcium sensitivity and abnormal expression of innate immunity genes precede dopaminergic defects in Pink1-deficient mice. *PLoS ONE* 6: e16038
- Amuthan G, Biswas G, Zhang SY, Klein-Szanto A, Vijayasathy C, Avadhani NG (2001) Mitochondria-to-nucleus stress signaling induces phenotypic changes, tumor progression and cell invasion. *EMBO J* 20: 1910–1920
- Annibaldi A, Meier P (2018) Checkpoints in TNF-induced cell death: implications in inflammation and cancer. *Trends Mol Med* 24: 49–65
- Bahat A, MacVicar T, Langer T (2021) Metabolism and innate immunity meet at the mitochondria. *Front Cell Dev Biol* 9: 720490
- Bhakar AL, Tannis LL, Zeindler C, Russo MP, Jobin C, Park DS, MacPherson S, Barker PA (2002) Constitutive nuclear factor-kappa B activity is required for central neuron survival. *J Neurosci* 22: 8466–8475
- Blondeau N, Widmann C, Lazdunski M, Heurteaux C (2001) Activation of the nuclear factor-kappaB is a key event in brain tolerance. *J Neurosci* 21: 4668–4677
- Bock FJ, Tait SWG (2020) Mitochondria as multifaceted regulators of cell death. *Nat Rev Mol Cell Biol* 21: 85–100
- Brenner D, Blaser H, Mak TW (2015) Regulation of tumour necrosis factor signalling: live or let die. *Nat Rev Immunol* 15: 362–374
- Cali T, Brini M (2021) Quantification of organelle contact sites by split-GFP-based contact site sensors (SPLICS) in living cells. *Nat Protoc* 16: 5287–5308
- Cervantes-Silva MP, Cox SL, Curtis AM (2021) Alterations in mitochondrial morphology as a key driver of immunity and host defence. *EMBO Rep* 22: e53086
- Cheng B, Christakos S, Mattson MP (1994) Tumor necrosis factors protect neurons against metabolic-excitotoxic insults and promote maintenance of calcium homeostasis. *Neuron* 12: 139–153
- Chowdhury A, Witte S, Aich A (2022) Role of mitochondrial nucleic acid sensing pathways in health and Patho-physiology. *Front Cell Dev Biol* 10: 796066
- Cieri D, Vicario M, Giacomello M, Vallese F, Filadi R, Wagner T, Pozzan T, Pizzo P, Scorrano L, Brini M et al (2018) SPLICS: a split green fluorescent protein-based contact site sensor for narrow and wide heterotypic organelle juxtaposition. *Cell Death Differ* 25: 1131–1145
- Cohen P, Strickson S (2017) The role of hybrid ubiquitin chains in the MyD88 and other innate immune signalling pathways. *Cell Death Differ* 24: 1153–1159
- Deas E, Plun-Favreau H, Gandhi S, Desmond H, Kjaer S, Loh SH, Renton AE, Harvey RJ, Whitworth AJ, Martins LM et al (2011) PINK1 cleavage at position A103 by the mitochondrial protease PARL. *Hum Mol Genet* 20: 867–879
- Desai R, East DA, Hardy L, Faccenda D, Rigon M, Crosby J, Alvarez MS, Singh A, Mainenti M, Hussey LK et al (2020) Mitochondria form contact sites with the nucleus to couple prosurvival retrograde response. *Sci Adv* 6: eabc9955
- Dittmar G, Winkhofer KF (2019) Linear ubiquitin chains: cellular functions and strategies for detection and quantification. *Front Chem* 7: 915
- Dresselhaus EC, Boersma MCH, Meffert MK (2018) Targeting of NF-kappaB to dendritic spines is required for synaptic signaling and spine development. *J Neurosci* 38: 4093–4103
- Eisenberg-Bord M, Schuldiner M (2017) Ground control to major TOM: mitochondria-nucleus communication. *FEBS J* 284: 196–210
- Eisenberg-Bord M, Zung N, Collado J, Drwesh L, Fenech EJ, Fadel A, Dezaorella N, Bykov YS, Rapaport D, Fernandez-Busnadiego R et al (2021) Cnm1 mediates nucleus-mitochondria contact site formation in response to phospholipid levels. *J Cell Biol* 220: e202104100
- Emmerich CH, Ordureau A, Strickson S, Arthur JS, Pedrioli PG, Komander D, Cohen P (2013) Activation of the canonical IKK complex by K63/M1-linked hybrid ubiquitin chains. *Proc Natl Acad Sci USA* 110: 15247–15252
- Emmerich CH, Bakshi S, Kellsall IR, Ortiz-Guerrero J, Shpiro N, Cohen P (2016) Lys63/Met1-hybrid ubiquitin chains are commonly formed during the activation of innate immune signalling. *Biochem Biophys Res Commun* 474: 452–461
- Exner N, Treske B, Paquet D, Holmstrom K, Schiesling C, Gispert S, Carballo-Carbajal I, Berg D, Hoepken HH, Gasser T et al (2007) Loss-of-function of human PINK1 results in mitochondrial pathology and can be rescued by parkin. *J Neurosci* 27: 12413–12418
- Fiesel FC, Ando M, Hudec R, Hill AR, Castanedes-Casey M, Caulfield TR, Moussaud-Lamodiere EL, Stankowski JN, Bauer PO, Lorenzo-Betancor O et al (2015) (Patho-)physiological relevance of PINK1-dependent ubiquitin phosphorylation. *EMBO Rep* 16: 1114–1130
- Fiil BK, Gyrd-Hansen M (2021) The Met1-linked ubiquitin machinery in inflammation and infection. *Cell Death Differ* 28: 557–569
- Fiil BK, Damgaard RB, Wagner SA, Keusekotten K, Fritsch M, Bekker-Jensen S, Mailand N, Choudhary C, Komander D, Gyrd-Hansen M (2013) OTULIN restricts Met1-linked ubiquitination to control innate immune signaling. *Mol Cell* 50: 818–830
- Fujita H, Rahighi S, Akita M, Kato R, Sasaki Y, Wakatsuki S, Iwai K (2014) Mechanism underlying IkkappaB kinase activation mediated by the linear ubiquitin chain assembly complex. *Mol Cell Biol* 34: 1322–1335
- Fuseya Y, Iwai K (2021) Biochemistry, pathophysiology, and regulation of linear ubiquitination: Intricate regulation by coordinated functions of the associated ligase and Deubiquitinase. *Cell* 10: 2706
- Gan ZY, Callegari S, Cobbold SA, Cotton TR, Mlodzianoski MJ, Schubert AF, Geoghegan ND, Rogers KL, Leis A, Dewson G et al (2022) Activation mechanism of PINK1. *Nature* 602: 328–335
- Giacomello M, Pyakurel A, Glytsou C, Scorrano L (2020) The cell biology of mitochondrial membrane dynamics. *Nat Rev Mol Cell Biol* 21: 204–224
- Goodall EA, Kraus F, Harper JW (2022) Mechanisms underlying ubiquitin-driven selective mitochondrial and bacterial autophagy. *Mol Cell* 82: 1501–1513
- Greene AW, Grenier K, Aguilera MA, Muise S, Farazifard R, Haque ME, McBride HM, Park DS, Fon EA (2012) Mitochondrial processing peptidase regulates PINK1 processing, import and parkin recruitment. *EMBO Rep* 13: 378–385
- Haas TL, Emmerich CH, Gerlach B, Schmukle AC, Cordier SM, Rieser E, Feltham R, Vince J, Warnken U, Wenger T et al (2009) Recruitment of the linear ubiquitin chain assembly complex stabilizes the TNF-R1 signaling complex and is required for TNF-mediated gene induction. *Mol Cell* 36: 831–844
- Hadian K, Griesbach RA, Dornauer S, Wanger TM, Nagel D, Metlitzky M, Beisker W, Schmidt-Suppran M, Krappmann D (2011) NEMO interaction with linear and K63 ubiquitin chains contributes to NF- $\kappa$ B activation. *J Biol Chem* 286: 26107–26117

- Harper JW, Ordureau A, Heo JM (2018) Building and decoding ubiquitin chains for mitophagy. *Nat Rev Mol Cell Biol* 19: 93–108
- Harper CS, White AJ, Lackner LL (2020) The multifunctional nature of mitochondrial contact site proteins. *Curr Opin Cell Biol* 65: 58–65
- Hayden MS, Ghosh S (2014) Regulation of NF- $\kappa$ B by TNF family cytokines. *Semin Immunol* 26: 253–266
- Henn IH, Bouman L, Schlehe JS, Schlierf A, Schramm JE, Wegener E, Nakaso K, Culmsee C, Berninger B, Krappmann D et al (2007) Parkin mediates neuroprotection through activation of I $\kappa$ B kinase/nuclear factor- $\kappa$ B signaling. *J Neurosci* 27: 1868–1878
- Hrdinka M, Fiil BK, Zucca M, Leske D, Bagola K, Yabal M, Elliott PR, Damgaard RB, Komander D, Jost PJ et al (2016) CYLD limits Lys63- and Met1-linked ubiquitin at receptor complexes to regulate innate immune signaling. *Cell Rep* 14: 2846–2858
- Huang da W, Sherman BT, Lempicki RA (2009a) Bioinformatics enrichment tools: paths toward the comprehensive functional analysis of large gene lists. *Nucleic Acids Res* 37: 1–13
- Huang da W, Sherman BT, Lempicki RA (2009b) Systematic and integrative analysis of large gene lists using DAVID bioinformatics resources. *Nat Protoc* 4: 44–57
- Jahan AS, Elbaek CR, Damgaard RB (2021) Met1-linked ubiquitin signalling in health and disease: Inflammation, immunity, cancer, and beyond. *Cell Death Differ* 28: 473–492
- Jin SM, Lazarou M, Wang C, Kane LA, Narendra DP, Youle RJ (2010) Mitochondrial membrane potential regulates PINK1 import and proteolytic destabilization by PARL. *J Cell Biol* 191: 933–942
- Kakade P, Ojha H, Raimi OG, Shaw A, Waddell AD, Ault JR, Burel S, Brockmann K, Kumar A, Ahangar MS et al (2022) Mapping of a N-terminal alpha-helix domain required for human PINK1 stabilization, Serine228 autophosphorylation and activation in cells. *Open Biol* 12: 210264
- Kane LA, Lazarou M, Fogel AI, Li Y, Yamano K, Sarraf SA, Banerjee S, Youle RJ (2014) PINK1 phosphorylates ubiquitin to activate parkin E3 ubiquitin ligase activity. *J Cell Biol* 205: 143–153
- Keusekotten K, Elliott PR, Glockner L, Fiil BK, Damgaard RB, Kulathu Y, Wauer T, Hospenthal MK, Cyrd-Hansen M, Krappmann D et al (2013) OTULIN antagonizes LUBAC signaling by specifically hydrolyzing Met1-linked polyubiquitin. *Cell* 153: 1312–1326
- Kirisako T, Kamei K, Murata S, Kato M, Fukumoto H, Kanie M, Sano S, Tokunaga F, Tanaka K, Iwai K (2006) A ubiquitin ligase complex assembles linear polyubiquitin chains. *EMBO J* 25: 4877–4887
- Komander D, Reyes-Turcu F, Licchesi JD, Odenwaelder P, Wilkinson KD, Barford D (2009) Molecular discrimination of structurally equivalent Lys 63-linked and linear polyubiquitin chains. *EMBO Rep* 10: 466–473
- Krappmann D, Patke A, Heissmeyer V, Scheidereit C (2001) B-cell receptor- and phorbol ester-induced NF- $\kappa$ B and c-Jun N-terminal kinase activation in B cells requires novel protein kinase C's. *Mol Cell Biol* 21: 6640–6650
- Kupka S, De Miguel D, Draber P, Martino L, Surinova S, Rittinger K, Walczak H (2016a) SPATA2-mediated binding of CYLD to HOIP enables CYLD recruitment to signaling complexes. *Cell Rep* 16: 2271–2280
- Kupka S, Reichert M, Draber P, Walczak H (2016b) Formation and removal of poly-ubiquitin chains in the regulation of tumor necrosis factor-induced gene activation and cell death. *FEBS J* 283: 2626–2639
- Lee HJ, Chung KC (2012) PINK1 positively regulates IL-1 $\beta$ -mediated signaling through Tollip and IRAK1 modulation. *J Neuroinflammation* 9: 271
- Lee HJ, Jang SH, Kim H, Yoon JH, Chung KC (2012) PINK1 stimulates interleukin-1 $\beta$ -mediated inflammatory signaling via the positive regulation of TRAF6 and TAK1. *Cell Mol Life Sci* 69: 3301–3315
- Lim GG, Chua DS, Basil AH, Chan HY, Chai C, Arumugam T, Lim KL (2015) Cytosolic PTEN-induced putative kinase 1 is stabilized by the NF- $\kappa$ B pathway and promotes non-selective mitophagy. *J Biol Chem* 290: 16882–16893
- Liu XY, Wei B, Shi HX, Shan YF, Wang C (2010) Tom70 mediates activation of interferon regulatory factor 3 on mitochondria. *Cell Res* 20: 994–1011
- Liu Y, Guardia-Laguarta C, Yin J, Erdjument-Bromage H, Martin B, James M, Jiang X, Przedborski S (2017) The ubiquitination of PINK1 is restricted to its mature 52-kDa form. *Cell Rep* 20: 30–39
- Lo YC, Lin SC, Rospigliosi CC, Conze DB, Wu CJ, Ashwell JD, Eliezer D, Wu H (2009) Structural basis for recognition of diubiquitins by NEMO. *Mol Cell* 33: 602–615
- Lork M, Verhelst K, Beyaert R (2017) CYLD, A20 and OTULIN deubiquitinases in NF- $\kappa$ B signaling and cell death: So similar, yet so different. *Cell Death Differ* 24: 1172–1183
- Matsumoto ML, Dong KC, Yu C, Phu L, Gao X, Hannoush RN, Hymowitz SG, Kirkpatrick DS, Dixit VM, Kelley RF (2012) Engineering and structural characterization of a linear polyubiquitin-specific antibody. *J Mol Biol* 418: 134–144
- Meffert MK, Chang JM, Wiltgen BJ, Fanselow MS, Baltimore D (2003) NF- $\kappa$ B functions in synaptic signaling and behavior. *Nat Neurosci* 6: 1072–1078
- Meissner C, Lorenz H, Weihofen A, Selkoe DJ, Lemberg MK (2011) The mitochondrial intramembrane protease PARL cleaves human Pink1 to regulate Pink1 trafficking. *J Neurochem* 117: 856–867
- Meschede J, Sadic M, Furthmann N, Miedema T, Sehr DA, Muller-Rischart AK, Bader V, Berlemann LA, Pils A, Schlierf A et al (2020) The parkin-coregulated gene product PACRG promotes TNF signaling by stabilizing LUBAC. *Sci Signal*: 13, eaav1256
- Mikenberg I, Widera D, Kaus A, Kaltschmidt B, Kaltschmidt C (2007) Transcription factor NF- $\kappa$ B is transported to the nucleus via cytoplasmic dynein/dynactin motor complex in hippocampal neurons. *PLoS ONE* 2: e589
- Misgeld T, Schwarz TL (2017) Mitostasis in neurons: maintaining mitochondria in an extended cellular architecture. *Neuron* 96: 651–666
- Montava-Garriga L, Ganley IG (2020) Outstanding questions in mitophagy: what we do and do not know. *J Mol Biol* 432: 206–230
- Muller-Rischart AK, Pils A, Beaudette P, Patra M, Hadian K, Funke M, Peis R, Deinlein A, Schweimer C, Kuhn PH et al (2013) The E3 ligase parkin maintains mitochondrial integrity by increasing linear ubiquitination of NEMO. *Mol Cell* 49: 908–921
- Neidl R, Schneider A, Bousiges O, Majchrzak M, Barbelivien A, de Vasconcelos AP, Dorgans K, Doussau F, Loeffler JP, Cassel JC et al (2016) Late-life environmental enrichment induces acetylation events and nuclear factor  $\kappa$ B-dependent regulations in the hippocampus of aged rats showing improved plasticity and learning. *J Neurosci* 36: 4351–4361
- Nguyen TN, Padman BS, Lazarou M (2016) Deciphering the molecular signals of PINK1/parkin mitophagy. *Trends Cell Biol* 26: 733–744
- Noad J, von der Malsburg A, Pathe C, Michel MA, Komander D, Rando F (2017) LUBAC-synthesized linear ubiquitin chains restrict cytosol-invading bacteria by activating autophagy and NF- $\kappa$ B. *Nat Microbiol* 2: 17063
- Nunnari J, Suomalainen A (2012) Mitochondria: in sickness and in health. *Cell* 148: 1145–1159
- Oikawa D, Sato Y, Ito H, Tokunaga F (2020) Linear ubiquitin code: its writer, erasers, decoders, inhibitors, and implications in disorders. *Int J Mol Sci* 21: 3381
- Ordureau A, Sarraf SA, Duda DM, Heo JM, Jedrychowski MP, Sviderskiy VO, Olszewski JL, Koerber JT, Xie T, Beausoleil SA et al (2014) Quantitative

- proteomics reveal a feedforward mechanism for mitochondrial PARKIN translocation and ubiquitin chain synthesis. *Mol Cell* 56: 360–375
- Ordureau A, Paulo JA, Zhang W, Ahfeldt T, Zhang J, Cohn EF, Hou Z, Heo JM, Rubin LL, Sidhu SS et al (2018) Dynamics of PARKIN-dependent mitochondrial ubiquitylation in induced neurons and model systems revealed by digital snapshot proteomics. *Mol Cell* 70: e8
- O'Riordan KJ, Huang IC, Pizzi M, Spano P, Boroni F, Egli R, Desai P, Fitch O, Malone L, Ahn HJ et al (2006) Regulation of nuclear factor kappaB in the hippocampus by group I metabotropic glutamate receptors. *J Neurosci* 26: 4870–4879
- Otten EG, Werner E, Crespillo-Casado A, Boyle KB, Dharamdasani V, Pathe C, Santhanam B, Randow F (2021) Ubiquitylation of lipopolysaccharide by RNF213 during bacterial infection. *Nature* 594: 111–116
- Pickles S, Vigie P, Youle RJ (2018) Mitophagy and quality control mechanisms in mitochondrial maintenance. *Curr Biol* 28: R170–R185
- Prinz WA, Toulmay A, Balla T (2020) The functional universe of membrane contact sites. *Nat Rev Mol Cell Biol* 21: 7–24
- Rahighi S, Ikeda F, Kawasaki M, Akutsu M, Suzuki N, Kato R, Kensche T, Uejima T, Bloor S, Komander D et al (2009) Specific recognition of linear ubiquitin chains by NEMO is important for NF-kappaB activation. *Cell* 136: 1098–1109
- Rasool S, Soya N, Truong L, Croteau N, Lukacs GL, Trempe JF (2018) PINK1 autophosphorylation is required for ubiquitin recognition. *EMBO Rep* 19: e44981
- Rasool S, Veyron S, Soya N, Eldeeb MA, Lukacs GL, Fon EA, Trempe JF (2022) Mechanism of PINK1 activation by autophosphorylation and insights into assembly on the TOM complex. *Mol Cell* 82: 44–59.e6
- Rehwinkel J, Gack MU (2020) RIG-I-like receptors: their regulation and roles in RNA sensing. *Nat Rev Immunol* 20: 537–551
- Rivkin E, Almeida SM, Ceccarelli DF, Juang YC, MacLean TA, Srikumar T, Huang H, Dunham WH, Fukumura R, Xie G et al (2013) The linear ubiquitin-specific deubiquitinase gumbly regulates angiogenesis. *Nature* 498: 318–324
- Salles A, Boccia M, Blake M, Corbi N, Passananti C, Baratti CM, Romano A, Freudenthal R (2015) Hippocampal dynamics of synaptic NF-kappa B during inhibitory avoidance long-term memory consolidation in mice. *Neuroscience* 291: 70–80
- Sauve V, Sung G, MacDougall EJ, Kozlov G, Saran A, Fakhri R, Fon EA, Gehring K (2022) Structural basis for feedforward control in the PINK1/parkin pathway. *EMBO J* 41: e109460
- Schwarz TL (2013) Mitochondrial trafficking in neurons. *Cold Spring Harb Perspect Biol* 5: a011304
- Scorrano L, De Matteis MA, Emr S, Giordano F, Hajnoczky G, Kornmann B, Lackner LL, Levine TP, Pellegrini L, Reinisch K et al (2019) Coming together to define membrane contact sites. *Nat Commun* 10: 1287
- Seth RB, Sun L, Ea CK, Chen ZJ (2005) Identification and characterization of MAVS, a mitochondrial antiviral signaling protein that activates NF-kappaB and IRF 3. *Cell* 122: 669–682
- Sha D, Chin LS, Li L (2010) Phosphorylation of parkin by Parkinson disease-linked kinase PINK1 activates parkin E3 ligase function and NF-kappaB signaling. *Hum Mol Genet* 19: 352–363
- Shi G, Lee JR, Grimes DA, Racacho L, Ye D, Yang H, Ross OA, Farrer M, McQuibban GA, Bulman DE (2011) Functional alteration of PARL contributes to mitochondrial dysregulation in Parkinson's disease. *Hum Mol Genet* 20: 1966–1974
- Shibata Y, Komander D (2022) Lubac. *Curr Biol* 32: R506–R508
- Shrum CK, Defrancisco D, Meffert MK (2009) Stimulated nuclear translocation of NF-kappaB and shuttling differentially depend on dynein and the dyactin complex. *Proc Natl Acad Sci USA* 106: 2647–2652
- Sima S, Barkovits K, Marcus K, Schmauder L, Hacker SM, Hellwig N, Morgner N, Richter K (2021) HSP-90/kinase complexes are stabilized by the large PPIase FKB-6. *Sci Rep* 11: 12347
- Spit M, Rieser E, Walczak H (2019) Linear ubiquitination at a glance. *J Cell Sci* 132: jcs208512
- Stangl A, Elliott PR, Pinto-Fernandez A, Bonham S, Harrison L, Schaub A, Kutzner K, Keusekotten K, Pfluger PT, El Oualid F et al (2019) Regulation of the endosomal SNX27-retromer by OTULIN. *Nat Commun* 10: 4320
- Stieglitz B, Morris-Davies AC, Koliopoulos MG, Christodoulou E, Rittinger K (2012) LUBAC synthesizes linear ubiquitin chains via a thioester intermediate. *EMBO Rep* 13: 840–846
- Sun S, Elwood J, Greene WC (1996) Both amino- and carboxyl-terminal sequences within I kappa B alpha regulate its inducible degradation. *Mol Cell Biol* 16: 1058–1065
- Thorne LG, Bouhaddou M, Reuschl AK, Zuliani-Alvarez L, Polacco B, Pelin A, Batra J, Whelan MVX, Hosmillo M, Fossati A et al (2022) Evolution of enhanced innate immune evasion by SARS-CoV-2. *Nature* 602: 487–495
- Tiku V, Tan MW, Dikic I (2020) Mitochondrial functions in infection and immunity. *Trends Cell Biol* 30: 263–275
- Tokunaga F, Ikeda F (2022) Linear ubiquitination in immune and neurodegenerative diseases, and beyond. *Biochem Soc Trans* 50: 799–811
- Tokunaga F, Sakata S, Saeki Y, Satomi Y, Kirisako T, Kamei K, Nakagawa T, Kato M, Murata S, Yamaoka S et al (2009) Involvement of linear polyubiquitylation of NEMO in NF-kappaB activation. *Nat Cell Biol* 11: 123–132
- Turrin NP, Rivest S (2006) Tumor necrosis factor alpha but not interleukin 1 beta mediates neuroprotection in response to acute nitric oxide excitotoxicity. *J Neurosci* 26: 143–151
- Tyanova S, Temu T, Cox J (2016) The MaxQuant computational platform for mass spectrometry-based shotgun proteomics. *Nat Protoc* 11: 2301–2319
- Vallese F, Catoni C, Cieri D, Barazzuol L, Ramirez O, Calore V, Bonora M, Giamogante F, Pinton P, Brini M et al (2020) An expanded palette of improved SPLICS reporters detects multiple organelle contacts *in vitro* and *in vivo*. *Nat Commun* 11: 6069
- Van Humbeek C, Cornelissen T, Hofkens H, Mandemakers W, Gevaert K, De Strooper B, Vandenberghe W (2011) Parkin interacts with ambra1 to induce mitophagy. *J Neurosci* 31: 10249–10261
- Varfolomeev E, Vucic D (2018) Intracellular regulation of TNF activity in health and disease. *Cytokine* 101: 26–32
- Verboom L, Hoste E, van Loo G (2021) OTULIN in NF-kappaB signaling, cell death, and disease. *Trends Immunol* 42: 590–603
- Wagner SA, Satpathy S, Beli P, Choudhary C (2016) SPATA2 links CYLD to the TNF-alpha receptor signaling complex and modulates the receptor signaling outcomes. *EMBO J* 35: 1868–1884
- Walker BR, Moraes CT (2022) Nuclear-mitochondrial interactions. *Biomolecules* 12: 427
- Wauer T, Swatek KN, Wagstaff JL, Gladkova C, Pruneda JN, Michel MA, Gersch M, Johnson CM, Freund SM, Komander D (2015) Ubiquitin Ser65 phosphorylation affects ubiquitin structure, chain assembly and hydrolysis. *EMBO J* 34: 307–325
- Weinberg SE, Sena LA, Chandel NS (2015) Mitochondria in the regulation of innate and adaptive immunity. *Immunity* 42: 406–417
- Weinelt N, van Wijk SJL (2021) Ubiquitin-dependent and -independent functions of OTULIN in cell fate control and beyond. *Cell Death Differ* 28: 493–504
- van Well EM, Bader V, Patra M, Sanchez-Vicente A, Meschede J, Furthmann N, Schnack C, Blusch A, Longworth J, Petrasch-Parwez E et al (2019) A protein quality control pathway regulated by linear ubiquitination. *EMBO J* 38: e100730

- Whitworth AJ, Pallanck LJ (2017) PINK1/parkin mitophagy and neurodegeneration-what do we really know *in vivo*? *Curr Opin Genet Dev* 44: 47–53
- Whitworth AJ, Lee JR, Ho VM, Flick R, Chowdhury R, McQuibban GA (2008) Rhomboid-7 and HtrA2/Omi act in a common pathway with the Parkinson's disease factors Pink1 and parkin. *Dis Model Mech* 1: 168–174; discussion 173
- van Wijk SJL, Fricke F, Herhaus L, Gupta J, Hotte K, Pampaloni F, Grumati P, Kaulich M, Sou YS, Komatsu M *et al* (2017) Linear ubiquitination of cytosolic *Salmonella typhimurium* activates NF-kappaB and restricts bacterial proliferation. *Nat Microbiol* 2: 17066
- Wikstrom JD, Katzman SM, Mohamed H, Twig G, Graf SA, Heart E, Molina AJ, Corkey BE, de Vargas LM, Danial NN *et al* (2007) Beta-cell mitochondria exhibit membrane potential heterogeneity that can be altered by stimulatory or toxic fuel levels. *Diabetes* 56: 2569–2578
- Yamano K, Youle RJ (2013) PINK1 is degraded through the N-end rule pathway. *Autophagy* 9: 1758–1769
- Yamano K, Kikuchi R, Kojima W, Hayashida R, Koyano F, Kawawaki J, Shoda T, Demizu Y, Naito M, Tanaka K *et al* (2020) Critical role of mitochondrial ubiquitination and the OPTN-ATG9A axis in mitophagy. *J Cell Biol* 219: e201912144
- Youle RJ (2019) Mitochondria-striking a balance between host and endosymbiont. *Science* 365: eaaw9855



**License:** This is an open access article under the terms of the [Creative Commons Attribution-NonCommercial-NoDerivs](https://creativecommons.org/licenses/by-nc-nd/4.0/) License, which permits use and distribution in any medium, provided the original work is properly cited, the use is non-commercial and no modifications or adaptations are made.